Chapter

1

Spectroscopy of Rocks and Minerals, and Principles of Spectroscopy

Roger N. Clark
U.S. Geological Survey
Denver, Colorado

1.1 INTRODUCTION

1.1.1 About This Chapter

Spectroscopy is the study of light as a function of wavelength that has been emitted, reflected, or scattered from a solid, liquid, or gas. In this chapter I discuss primarily the spectroscopy of minerals, but the principles apply to any material. No single chapter can cover this topic adequately, and one could argue, not even a single book. Thus, in some ways, this chapter may fall short of some reader's expectations. This chapter constitutes an overview of what is already known (some of which may be covered better in other reviews) and some of the practical lessons of spectroscopy, some of which have been in use by spectroscopists as common knowledge but have not necessarily been published previously in detail. See Farmer (1974), Adams (1975), Hunt (1977, 1982), Clark and Roush (1984), Clark et al. (1990a), Gaffey et al. (1993), Salisbury (1993), and references in those papers for more details.

1.1.2 Absorption and Scattering

As photons enter a mineral, some are reflected from grain surfaces, some pass through the grain, and some are absorbed. Those photons that are reflected from grain sur-

Remote Sensing for the Earth Sciences: Manual of Remote Sensing, 3 ed., Vol. 3, edited by Andrew N. Rencz.
ISBN: 0471-29405-5

faces or refracted through a particle are said to be *scattered*. Scattered photons may encounter another grain or be scattered away from the surface so they may be detected and measured. Photons may also originate from a surface, a process called *emission*. All natural surfaces emit photons when they are above absolute zero. Emitted photons are subject to the same physical laws of reflection, refraction, and absorption to which incident photons are bound.

Photons are absorbed in minerals by several processes. The variety of absorption processes and their wavelength dependence allow us to derive information about the chemistry of a mineral from its reflected or emitted light. The human eye is a crude reflectance spectrometer: We can look at a surface and see color. Our eyes and brain are processing the wavelength-dependent scattering of visible-light photons to reveal something about what we are observing, such as the red color of hematite or the green color of olivine. A modern spectrometer, however, can measure finer details over a broader wavelength range and with greater precision. Thus a spectrometer can measure absorptions due to more processes than can be seen with the eye.

1.1.3 Spectroscopy Terms

There are four general parameters that describe the capability of a spectrometer: (1) spectral range, (2) spectral bandwidth, (3) spectral sampling, and (4) signal/noise ratio. Spectral range is important to cover enough diagnostic spectral absorptions to solve a desired problem. There are general spectral ranges that are in common use, each to first order controlled by detector technology: (1) ultraviolet (UV): 0.001 to 0.4 μm, (2) visible: 0.4 to 0.7 μm, (3) near-infrared (NIR): 0.7 to 3.0 μm, (4) mid-infrared (MIR): 3.0 to 30 μm, and (5) far infrared (FIR): 30 μm to 1 mm (see, e.g., the *Photonics Design and Applications Handbook*, 1996 and the *Handbook of Chemistry and Physics*, any recent year). The approximate wavelength range 0.4 to 1.0 μm is sometimes referred to in the remote sensing literature as the VNIR (for visible/near-infrared: 0.4 to 1.0 μm), and the range 1.0 to 2.5 μm is sometimes referred to as the SWIR (shortwave-infrared). It should be noted that these terms are not recognized standard terms in fields other than remote sensing, and because the NIR in VNIR conflicts with the accepted NIR range, the VNIR and SWIR terms probably should be avoided. The mid-infrared covers thermally emitted energy, which for the Earth starts at about 2.5 to 3 μm, peaking near 10 μm, decreasing beyond the peak, with a shape controlled by gray-body emission.

Spectral bandwidth is the width of an individual spectral channel in the spectrometer. The narrower the spectral bandwidth, the narrower the absorption feature the spectrometer will measure accurately, if enough adjacent spectral samples are obtained. Some systems have a few broad channels, not contiguously spaced, and thus are not considered spectrometers (Figure 1.1*a*), Examples include the *Landsat* thematic mapper (TM) system and the moderate resolution imaging spectroradiometer (MODIS), which cannot resolve narrow absorption features. Others, such as the NASA JPL airborne visual/infrared imaging spectrometer (AVIRIS) system, have many narrow bandwidths, contiguously spaced (Figure 1.1*b*). Figure 1.1 shows spectra for the mineral alunite that could be obtained by some broadband and spectrometer systems. Note the loss in subtle spectral detail in the lower-resolution systems compared to the laboratory spectrum. Bandwidths and sampling greater than 25 nm rapidly lose the ability to resolve important mineral absorption features. All the

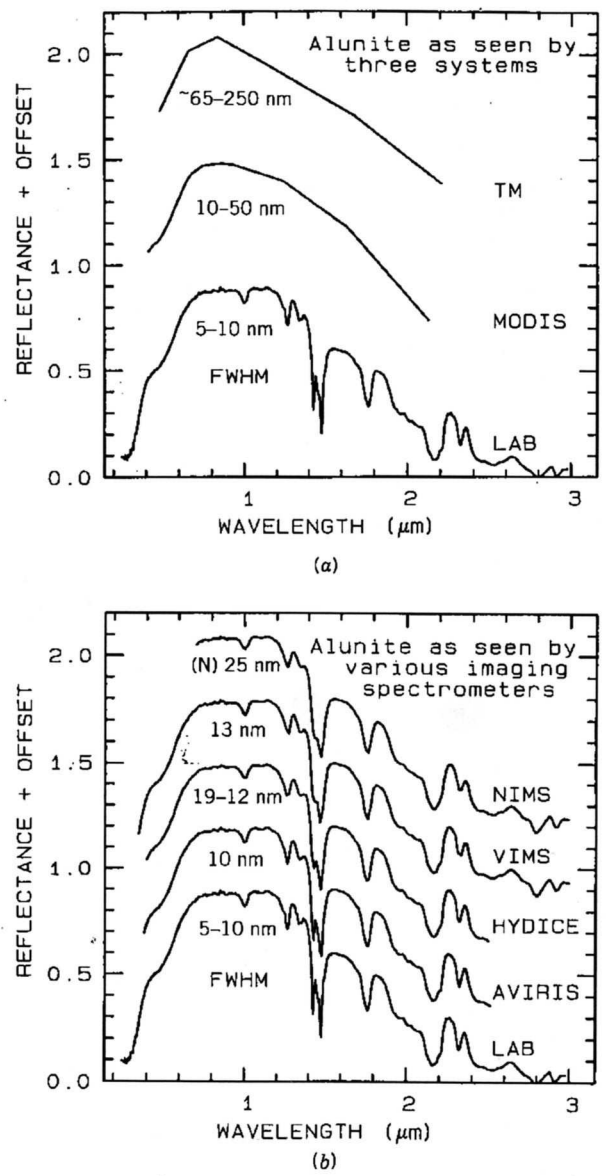

Figure 1.1 Spectra of the mineral alunite shown as measured in the laboratory and for (*a*) broadband remote sensing instruments and (*b*) some imaging spectrometers (see the text). The FWHM is the full width at half maximum, defined in Figure 1.2. The alunite is sample HS295.3B from the USGS spectral library (Clark et al., 1993b). *Note*: The NIMS and VIMS systems measure to 5 μm. Each spectrum is offset upward (*a*) 0.6 unit and (*b*) 0.3 unit from the one below it, for clarity.

spectra in Figure 1.1*b* are sampled at half-Nyquist (critical sampling) except the near-infrared mapping spectrometer (NIMS), which is at Nyquist sampling. Note, however, that the fine details of the absorption features are lost at about the 25-nm bandpass of NIMS. For example, the shoulder in the 2.2-μm absorption band is lost at 25-nm bandpass. The visual and infrared mapping spectrometer (VIMS) and NIMS systems measure out to 5 μm, thus can see absorption bands not obtainable by the other systems.

The shape of the bandpass profile is also important. Ideally, each spectrometer channel rejects all light except that from within a given narrow-wavelength range, but occasionally, due to optical effects too complex to discuss in detail here, light may leak in from out of the bandpass (e.g., scattering within the optical system, or inadequate blocking filters). The most common bandpass in spectrometers is a Gaussian profile. While specific spectrometer designs may have well-defined theoretical bandpass profiles, aberrations in the optical system usually smears the profile closer to a Gaussian shape. The width of the bandpass is usually defined as the width in wavelength at the 50% response level of the function, as shown in Figure 1.2, called the *full width at half maximum* (FWHM).

Spectral sampling is the distance in wavelength between the spectral bandpass profiles for each channel in the spectrometer as a function of wavelength. Spectral sampling is often confused with bandpass, with the two lumped together and called *resolution*. Information theory tells us that to resolve two spectral features, we must have two samples. Further, in order not to introduce sampling bias, the samples must be close enough together to measure the peak and valley locations. The Nyquist theorem states that the maximum information is obtained by sampling at one-half the FWHM. Spectrometer design, however, sometimes dictates a different sampling, and many modern spectrometers in use (e.g., AVIRIS, VIMS) sample at half-Nyquist, a sampling interval approximately equal to the FWHM. Note that the AVIRIS system has a bandpass of about 0.01 μm (10 nm), a sampling of about 0.01 μm, and thus

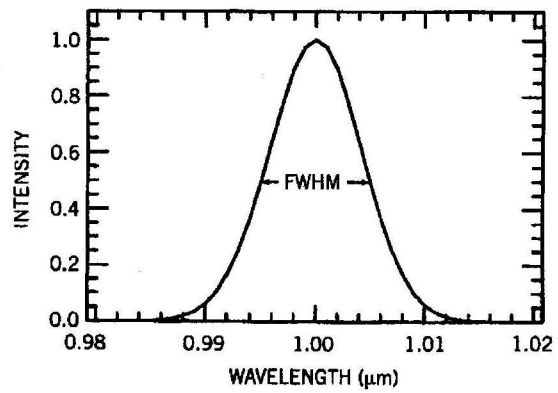

Figure 1.2 Gaussian profile with a full width at half maximum (FWHM) of 10 nm. This profile is typical of spectrometers such as AVIRIS, which has 224 such profiles spaced at about 10 nm.

a spectral resolution of about 0.02 μm (20 nm). The NIMS system in Figure 1.1 can sample at Nyquist (shown), half-Nyquist, and lower.

Finally, a spectrometer must measure the spectrum with enough precision to record details in the spectrum. The signal/noise ratio (S/N) required to solve a particular problem will depend on the strength of the spectral features under study. S/N is dependent on the detector sensitivity, spectral bandwidth, and intensity of the light reflected or emitted from the surface being measured. A few spectral features are quite strong and a S/N value of only about 10 will be adequate to identify them; whereas others are weak, and a S/N value of several hundred (and higher) is often needed (Swayze et al., submitted).

1.1.4 Imaging Spectroscopy

Today, spectrometers are in use in the laboratory, in the field, in aircraft (looking both down at the Earth and up into space), and on satellites. Reflectance and emittance spectroscopy of natural surfaces are sensitive to specific chemical bonds in materials, whether solid, liquid, or gas. Spectroscopy has the advantage of being sensitive to both crystalline and amorphous materials, unlike some diagnostic methods, such as x-ray diffraction. Spectroscopy's other main advantage is that it can be used up close (e.g., in the laboratory) to far away (e.g., to look down on the Earth or up at other planets). Spectroscopy's historical disadvantage is that it is too sensitive to small changes in the chemistry and/or structure of a material. The variations in material composition often cause shifts in the position and shape of absorption bands in the spectrum. Thus, with the vast variety of chemistry typically encountered in the real world, spectral signatures can be quite complex and sometimes unintelligible. However, that is now changing, with increased knowledge of the natural variation in spectral features and the causes of the shifts, so that the previous disadvantage is turning into a huge advantage, allowing us to probe ever more detail about the chemistry of our natural environment.

With the advance in computer and detector technology, the new field of imaging spectroscopy is developing (Goetz et al., 1985; Green et al., 1990; Vane et al., 1993; Chapter 5; Chapter 11; and references therein). Imaging spectroscopy is a new technique for obtaining a spectrum in each position of a large array of spatial positions so that any one spectral wavelength can be used to make a recognizable image. The image might be of a rock in the laboratory, a field study site from an aircraft, or an entire planet from a spacecraft or Earth-based telescope. By analyzing the spectral features, and thus specific chemical bonds in materials, one can map where those bonds occur, and thus map materials. Such mapping is best done by spectral feature analysis.

Imaging spectroscopy has many names in the remote sensing community, including *imaging spectrometry*, *hyperspectral*, and *ultraspectral imaging*. *Spectroscopy* is the study of electromagnetic radiation. *Spectrometry* is derived from *spectrophotometry*, the measure of photons as a function of wavelength, a term used for years in astronomy. However, spectrometry is used increasingly to indicate the measurement of nonlight quantities, such as in mass spectrometry (e.g., Ball, 1995). *Hyper* means excessive, but no imaging spectrometer in use can be considered hyperspectral—after all, a couple of hundred channels pales in comparison to a truly high-resolution

spectrometer with millions of channels. *Ultraspectral* is beyond hyperspectral, a lofty goal that we have not yet reached. Terms such as *laboratory spectrometer, spectroscopist, reflectance spectroscopy,* and *thermal emission spectroscopy* are in common use. One rarely, if ever, sees the converse: *spectrometrist, reflectance spectrometry,* and so on. So it seems prudent to keep the terminology consistent with *imaging spectroscopy.*

This chapter provides an introduction to the factors affecting the spectra of natural materials, including scattering and absorption, and the causes of absorption features. We also discuss doing quantitative estimates of mixtures and show sample spectra of minerals and other common materials that might be encountered in the natural world.

1.1.5 Atmospheric Transmittance: Windows for Remote Sensing

Any effort to measure the spectral properties of a material through a planetary atmosphere must consider where the atmosphere absorbs. For example, the Earth's atmospheric transmittance is shown in Figure 1.3. The drop toward the ultraviolet is due to scattering and strong ozone absorption at wavelengths short of 0.35 μm. Ozone also displays an absorption at 9.6 μm. Oxygen absorbs at 0.76 μm in a narrow feature. CO_2 absorbs at 2.01 and 2.06, with a weak doublet near 1.6 μm. Water causes most of the rest of the absorption throughout the spectrum and hides additional (weaker) absorptions from other gases. The mid-infrared spectrum in Figure 1.3*b* shows the effect of doubling CO_2, which in this case is small compared to the absorption due to water. Although we will see that the spectral region near 1.4 and 3 μm can be diagnostic of OH-bearing minerals, we cannot usually use these wavelengths when remotely measuring spectra through the Earth's atmosphere (it has been done from high-elevation observatories during dry weather conditions). However, these spectral regions can be used in the laboratory where the atmospheric path lengths are thousands of times smaller or when measuring spectra of other planets from orbiting spacecraft.

1.2 REFLECTION AND ABSORPTION PROCESSES

1.2.1 Reflection and Absorption

When a stream of photons encounter a medium with a change in the index of refraction, some are reflected and some are refracted into the medium. It is beyond this chapter to review all the physical laws of reflection and refraction; a good optics or physics book can do that (e.g., Hecht, 1987). However, the basics of reflection should be understood. All materials have a complex index of refraction:

$$m = n - jK \tag{1.1}$$

where m is the complex index of refraction, n is the real part of the index, $j = (-1)^{1/2}$, and K is the imaginary part of the index of refraction, sometimes called the extinction coefficient.

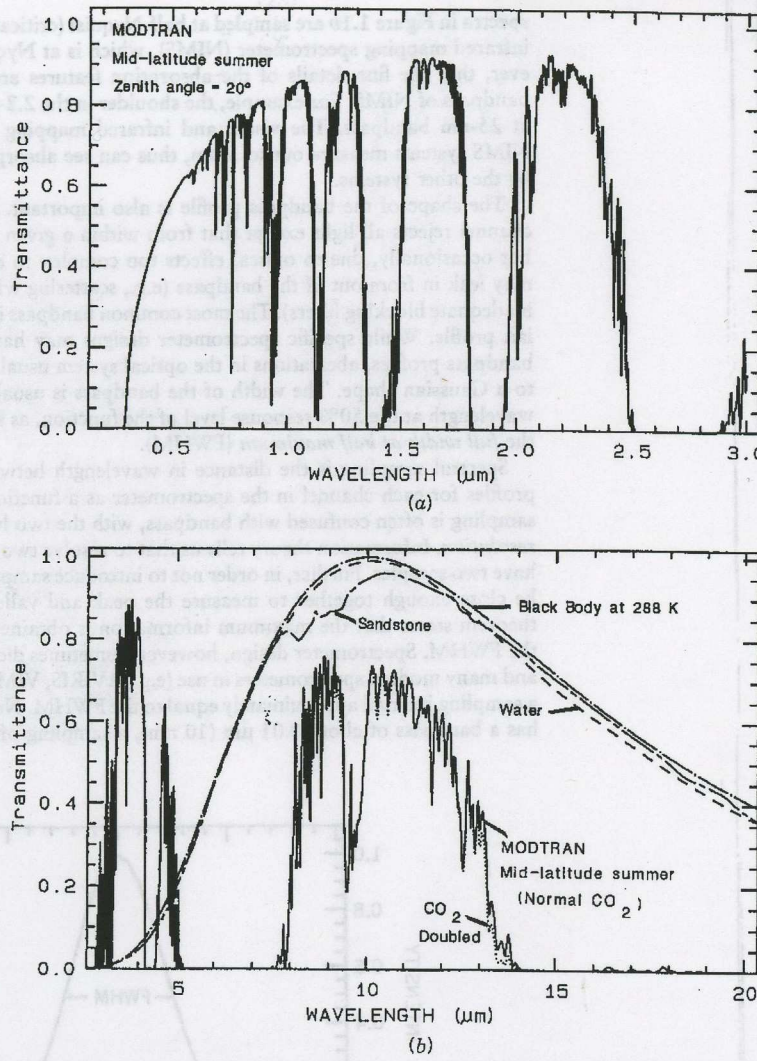

Figure 1.3 (*a*) Modtran (Berk et al., 1989) modeled atmospheric transmittance, visible to near-infrared. Most of the absorptio are due to water. Oxygen occurs at 0.76 μm, carbon dioxide at 2.0 and 2.06 μm. (*b*) Atmospheric transmittance, mid-infrar is compared to scaled gray-body spectra. Most of the absorption is due to water. Carbon dioxide has a strong 15-μm ba and the dotted line shows the increased absorption due to doubling CO_2. Also shown is the blackbody emission at 288 K a the gray-body emission from water and a sandstone scaled to fit on this transmittance scale. The water and sandstone curv were computed from reflectance data using 1 − reflectance × a blackbody at 288 K.

When photons enter an absorbing medium, they are absorbed according to *Beer's law:*

$$I = I_o e^{-kx} \tag{1.2}$$

where I is the observed intensity, I_o is the original light intensity, k an absorption coefficient, and x the distance traveled through the medium.

The absorption coefficient is related to the complex index of refraction by the equation:

$$k = \frac{4\pi K}{\lambda} \tag{1.3}$$

where λ is the wavelength of light. A sample index of refraction, n, and extinction coefficient, K, are shown in Figure 1.4*a* for quartz. The reflection of light, R, normally incident onto a plane surface is described by the *Fresnel equation:*

$$R = \frac{(n-1)^2 + K^2}{(n+1)^2 + K^2} \tag{1.4}$$

At angles other than normal, the reflectance is a complex trigonometric function involving the polarization direction of the incident beam and is left to the reader to study in standard optics or physics textbooks. The reflection from quartz grains as measured on a laboratory spectrometer is shown in Figure 1.4*b*. While the spectrum is of a particulate surface, first surface reflection dominates all wavelengths and so is similar to the spectrum of a slab of quartz.

The absorption coefficient is traditionally expressed in units of cm^{-1} and x in cm. Equations (1.1) to (1.4) hold for a single wavelength. At other wavelengths, the absorption coefficient and index of refraction are different, and the reflected intensity observed varies. The absorption coefficient as a function of wavelength is a fundamental parameter describing the interaction of photons with a material. So is the index of refraction, but it generally varies less than the absorption coefficient as a function of wavelength, especially at visible and near-infrared wavelengths. At fundamental absorption bands, both n and K vary strongly with wavelength, as shown in Figure 1.4*a*, although K still varies over more orders of magnitude than n does.

The complex index of refraction in Figure 1.4*a* shows important properties of materials. As one moves to longer wavelengths (left to right in Figure 1.4*a*), the index of refraction decreases to a minimum just before a sharp rise (e.g., at 8.5 and 12.6 μm in Figure 1.4*a*). The minimum is often near or even below $n = 1$. The wavelength where $n = 1$, called the *Christensen frequency*, usually results in a minimum in reflected light because of the small (to zero) difference in the index of refraction compared to the surrounding medium (e.g., air or vacuum). The location of the observed reflectance minimum is also controlled by the extinction coefficient according to equation (1.4). Note that the Christensen frequency sometimes occurs at a wavelength shorter than the maximum in the extinction coefficient (e.g., Figure 1.4*a*). This maximum is called the *reststrahlen band:* the location of fundamental vibrational stretching modes in the near and mid-infrared. The combination of n and K

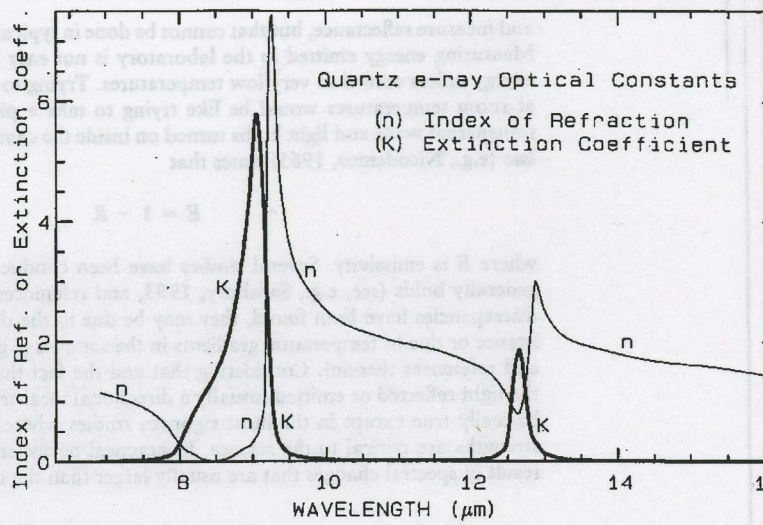

(*a*)

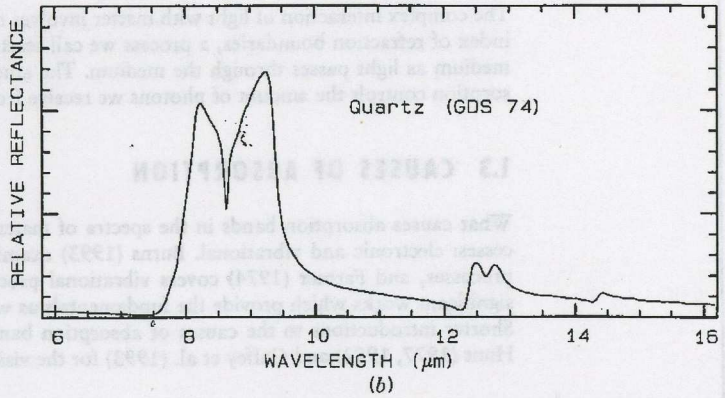

(*b*)

Figure 1.4 (*a*) Optical constants of quartz, SiO_2 (from Spitzer and Kleinman, 1960); (*b*) relative reflectance of powde quartz.

at these wavelengths often results in high reflectance. See Hapke (1993) for mo details.

1.2.2 Emittance

At mid-infrared wavelengths, materials normally receive thermally emitted photo In the laboratory one can shine enough light on a sample to ignore emitted photo

and measure reflectance, but that cannot be done in typical remote sensing situations. Measuring energy emitted in the laboratory is not easy because all materials emit energy unless cooled to very low temperatures. Trying to measure thermal emission at room temperatures would be like trying to take a picture with a camera with transparent walls and light bulbs turned on inside the camera! However, *Kirchhoff's law* (e.g., Nicodemus, 1965) states that

$$E = 1 - R \tag{1.5}$$

where E is emissivity. Several studies have been conducted to show that the rule generally holds (see, e.g., Salisbury, 1993, and references therein). Although some discrepancies have been found, they may be due to the difficulty of measuring emittance or due to temperature gradients in the samples (e.g., Henderson et al., 1996, and references therein). Considering that and the fact that one rarely measures all the light reflected or emitted (usually a directional measurement is made), the law is basically true except in the most rigorous studies where absolute levels and band strengths are critical to the science. In practical terms, small changes in grain size result in spectral changes that are usually larger than the discrepancies in the law.

1.2.3 Summary

The complex interaction of light with matter involves reflection and refraction from index of refraction boundaries, a process we call scattering, and absorption by the medium as light passes through the medium. The amount of scattering versus absorption controls the amount of photons we receive from a surface.

1.3 CAUSES OF ABSORPTION

What causes absorption bands in the spectra of materials? There are general processes: electronic and vibrational. Burns (1993) examines the details of electronic processes, and Farmer (1974) covers vibrational processes. These two books are significant works which provide the fundamentals as well as practical information. Shorter introductions to the causes of absorption bands in minerals are given by Hunt (1977, 1982) and Gaffey et al. (1993) for the visible and near-infrared.

1.3.1 Electronic Processes

Isolated atoms and ions have discrete energy states. Absorption of photons of a specific wavelength causes a change from one energy state to a higher-energy state. Emission of a photon occurs as a result of a change in an energy state to a lower-energy state. When a photon is absorbed, it is usually not emitted at the same wavelength. For example, it can cause heating of the material, resulting in gray-body emission at longer wavelengths.

In a solid, electrons may be shared between individual atoms. The energy level of shared electrons may become smeared over a range of values called *energy bands*.

However, bound electrons will still have quantized energy states (see, e.g., Burn 1970, 1993).

1.3.1.1 CRYSTAL FIELD EFFECTS.

The most common electronic process revealed in the spectra of minerals is due unfilled electron shells of transition elements (Ni, Cr, Co, Fe, etc.). Iron is the mo common transition element in minerals. For all transition elements, *d* orbitals ha identical energies in an isolated ion, but the energy levels split when the atom located in a crystal field (see, e.g., Burns, 1970, 1993). This splitting of the orbi energy states enables an electron to be moved from a lower level into a higher le by absorption of a photon having an energy matching the energy difference betwe the states. The energy levels are determined by the valence state of the atom (e. Fe^{2+}, Fe^{3+}), its coordination number, and the symmetry of the site it occupies. T levels are also influenced by the type of ligands formed, the extent of distortion the site, and the value of the metal–ligand interatomic distance (e.g., Burns, 199 The crystal field varies with crystal structure from mineral to mineral; thus t amount of splitting varies and the same ion (e.g., Fe^{2+}) produces obviously differe absorptions, making specific mineral identification possible from spectroscopy (Fi ures 1.5 to 1.7).

Example Fe^{2+} absorptions are shown in Figure 1.5*a* (olivines) and Figure 1. (pyroxenes). Note the shift in band position and shape between the different cor positions. Sample Fe^{3+} absorptions are shown in goethite (FeOOH) and hemati (Fe_2O_3) in Figure 1.7*a*. Compositional changes also shift vibrational absorption discussed below, and as seen in Figures 1.5*b*, 1.6*b*, and 1.7*b*. The composition shifts of the electronic absorptions have been studied by Adams (1974, 1975) ar Cloutis and Gaffey (1991) for pyroxenes and are shown in Figure 1.6*c*, and by Kir and Ridley (1987) for olivines.

The unfilled shells of rare earth ions involve deep-lying electrons that are we shielded from surrounding crystal fields, so the energy levels remain largely u changed. Thus absorption bands due to rare earth elements are not diagnostic mineralogy but of the presence of the ions in the mineral (Figure 1.8).

1.3.1.2 CHARGE TRANSFER ABSORPTIONS.

Absorption bands can also be caused by charge transfers, interelement transitio where the absorption of a photon causes an electron to move between ions or b tween ions and ligands. The transition can also occur between the same metal different valence states, such as between Fe^{2+} and Fe^{3+}. In general, absorption banc caused by charge transfers are diagnostic of mineralogy. Their strengths are typical hundreds to thousands of times stronger than those of crystal field transitions. Th band centers usually occur in the ultraviolet, with the wings of the absorption ex tending into the visible. Charge transfer absorptions are the main cause of the re color of iron oxides and hydroxides (Figure 1.7*a*). Morris et al. (1985) studied th details of submicron iron oxides, where it was found that the absorption banc decrease rapidly in intensity. This occurs because the increased surface/volume rati at small grain size results in a greater proportion of grain boundaries where cryst field effects are different, resulting in lower magnetic coupling and reduced absorp tion strength. Other iron oxides probably show similar effects. Reflectance spectr

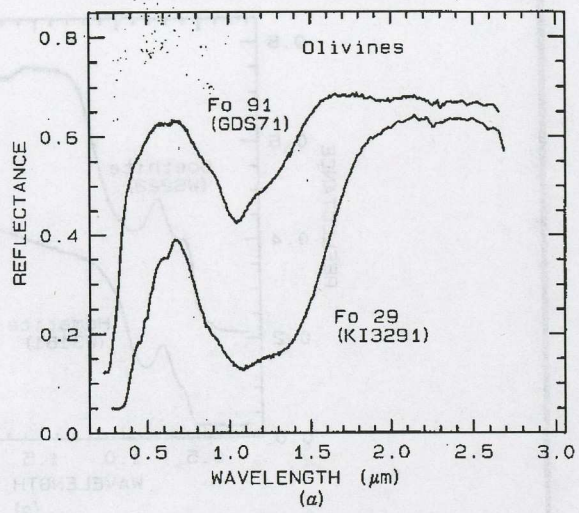

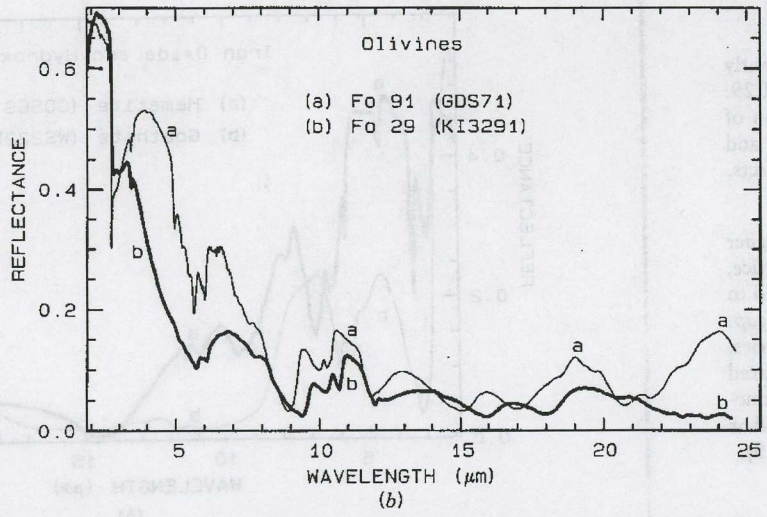

Figure 1.5 (*a*) Reflectance spectra of two olivines, showing the change in band position and shape with composition. The 1-μm absorption band is due to a crystal field absorption of Fe^{2+}. "Fo" stands for forsterite (Mg_2SiO_4) in the forsterite–fayalite ($Fe_2^{2+}SiO_4$) olivine solid solution series. The Fo 29 sample (KI3291 from King and Ridley, 1987) has an FeO content of 53.65%, while the Fo 91 sample (GDS 71; labeled Twin Sisters Peak in King and Ridley, 1987) has an FeO content of 7.93%. The mean grain size is 30 and 25 μm respectively. The 1-μm band position varies from about 1.08 μm at Fo 10 to 1.05 μm at Fo 90 (King and Ridley, 1987). (*b*) Same as for part (*a*) but for mid-infrared wavelengths. Note the shifts in the spectral features due to the change in composition. See the text for a discussion of vibrational absorption bands.

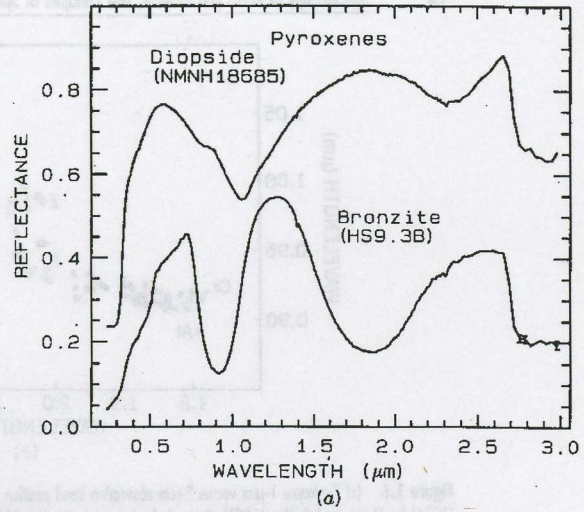

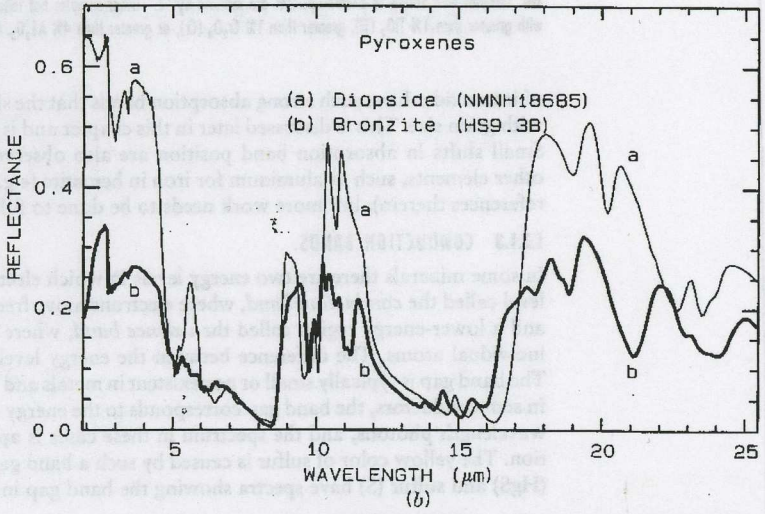

Figure 1.6 (*a*) Reflectance spectra of two pyroxenes, showing the change in Fe^{2+} absorption band position and shape with composition (from Clark et al., 1993b). Diopside, sample NMNH18685, is $CaMgSi_2O_6$, but some Fe^{2+} substitutes for Mg. Bronzite, sample HS9.3B, is $(Mg,Fe)SiO_3$ with mostly Mg. The 1-μm versus the 2-μm band position of a pyroxene describes the pyroxene composition [part (*c*)]. The diopside spectrum is offset 0.2 unit upward. (*b*) Same as for part (*a*) but for mid-infrared wavelengths. Note the shifts in the spectral features due to the change in composition.

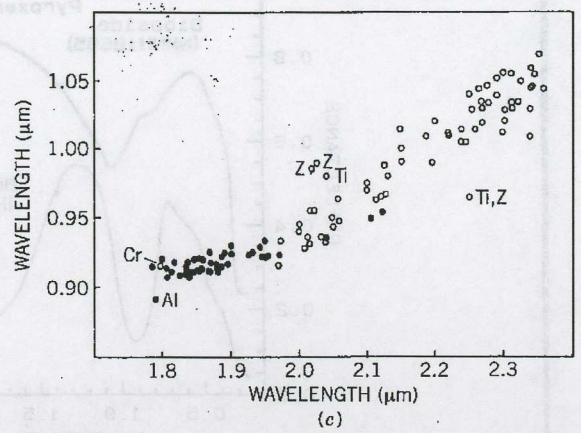

Figure 1.6 (*c*) Pyroxene 1-μm versus 2-μm absorption band position as a function of composition, as adapted from Adams (1974) by Cloutis and Gaffey (1991). Open circles have greater than 11% wollastonite (Wo), and solid symbols less than 11% Wo. Samples with zoned or exolved phases are marked by "Z." Other samples not following the "normal" trend include those with greater than 1% TiO_2 (Ti), greater than 1% Cr_2O_3 (Cr), or greater than 4% Al_2O_3. (From Cloutis and Gaffey, 1991.)

of iron oxides have such strong absorption bands that the shape changes significantly with grain size. This is discussed later in this chapter and is illustrated in Figure 1.29. Small shifts in absorption band position are also observed due to substitution of other elements, such as aluminum for iron in hematite (e.g., Morris et al., 1985, and references therein), but more work needs to be done to fully understand the effects.

1.3.1.3 CONDUCTION BANDS.

In some minerals there are two energy levels in which electrons may reside: a higher level called the *conduction band*, where electrons move freely throughout the lattice, and a lower-energy region called the *valence band*, where electrons are attached to individual atoms. The difference between the energy levels is called the *band gap*. The band gap is typically small or nonexistent in metals and is very large in dielectrics. In semiconductors, the band gap corresponds to the energy of visible to near-infrared wavelength photons, and the spectrum in these cases is approximately a step function. The yellow color of sulfur is caused by such a band gap. The minerals cinnabar (HgS) and sulfur (S) have spectra showing the band gap in the visible (Figure 1.9).

1.3.1.4 COLOR CENTERS.

A few minerals show color due to absorption by *color centers*. A color center is caused by irradiation (e.g., by solar ultraviolet radiation) of an imperfect crystal. Crystals in nature have lattice defects that disturb the periodicity of the crystal. For example, defects might be caused by impurities. These defects can produce discrete energy levels and electrons can become bound to them. The movement of an electron into the defect requires photon energy. The yellow, purple, and blue colors of fluorite are caused by color centers. See Hunt (1977) and references therein for more details.

More detailed discussions of electronic processes can be found in review papers

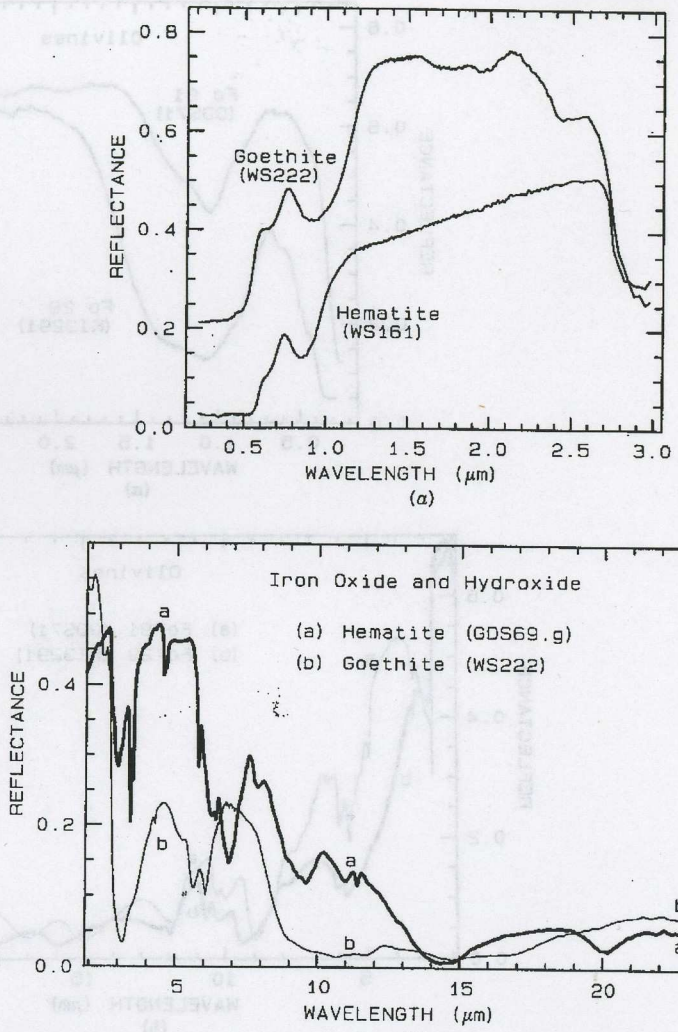

Figure 1.7 (*a*) Reflectance spectra of the iron oxide hematite (Fe_2O_3) and iron hydroxide goethite (FeOOH) (from Clark et al., 1993b). The intense charge transfer band in the ultraviolet (<0.4 μm) is "saturated" in reflectance, so only first surface (specular) reflection is seen in these spectra. The 0.9-and 0.86-μm absorption features are due to Laporte-forbidden transitions (e.g., Morris et al., 1985; Sherman, 1990; and references therein). The absorption at 2.7 to 3 μm is due to trace water in the samples, and in the case of goethite, the OH. The goethite spectrum is offset upward 0.2 unit. (*b*) Same as for part (*a*) but for mid-infrared wavelengths.

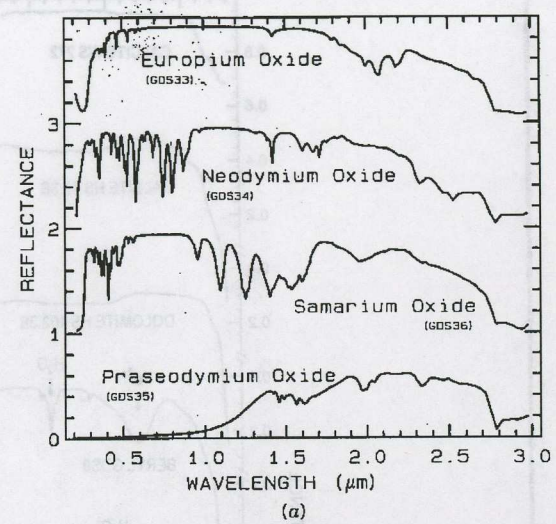

Figure 1.8 (*a*) Reflectance spectra of rare earth oxides. These absorptions are due to crystal field transitions involving deep-lying electrons of the rare earth element and do not shift when the rare earth ion is in another mineral. Each spectrum is offset by 1.0 unit, for clarity. (Spectra from Clark et al., 1993b.) (*b*) Same as for part (*a*) except showing absorptions in the visible region. Spectra are offset 1.0 unit for clarity. Spectral resolution is about 1 nm, critically sampled.

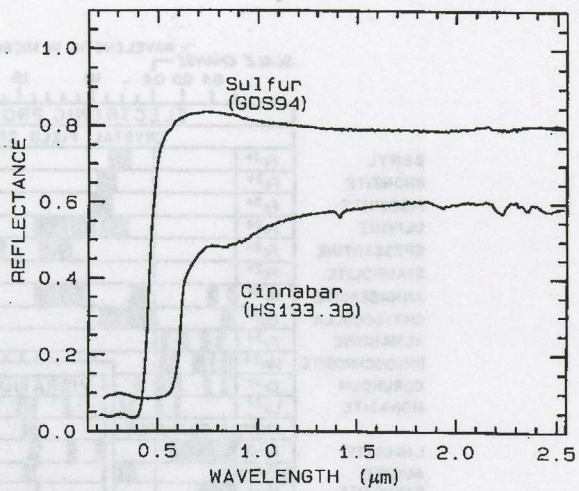

Figure 1.9 Reflectance spectra of sulfur, S, and cinnabar, HgS, showing conduction bands in the visible. (From Clark et 1993b.)

by Hunt (1977) and Gaffey et al. (1993) and in a book by Burns (1993). A summa diagram of the causes of absorption bands is shown in Figure 1.10.

1.3.2 Vibrational Processes

The bonds in a molecule or crystal lattice are like springs with attached weights: th entire system can vibrate. The frequency of vibration depends on the strength of eac spring (the bond in a molecule) and their masses (the mass of each element in molecule). For a molecule with N atoms, there are $3N - 6$ normal modes of vibra tions called *fundamentals*. Each vibration can also occur at roughly multiples of th original fundamental frequency. The additional vibrations are called *overtones* whe they involve multiples of a single fundamental mode, and *combinations* when the involve different modes of vibrations.

A vibrational absorption will be seen in the infrared spectrum only if the molecul responsible shows a dipole moment (it is said to be infrared active). A symmetri molecule such as N_2 is not normally infrared active unless it is distorted (e.g., whe under high pressure). Vibrations from two or more modes can occur at the sam frequency, and because they cannot be distinguished, are said to be degenerate. A isolated molecule with degenerate modes may show the modes at slightly diffe ent frequencies in a crystal because of the nonsymmetric influences of the cryst field.

A free molecule can rotate and move translationally, but even in a solid, partia rotation and slight translation can occur. These motions are called *lattice modes* an

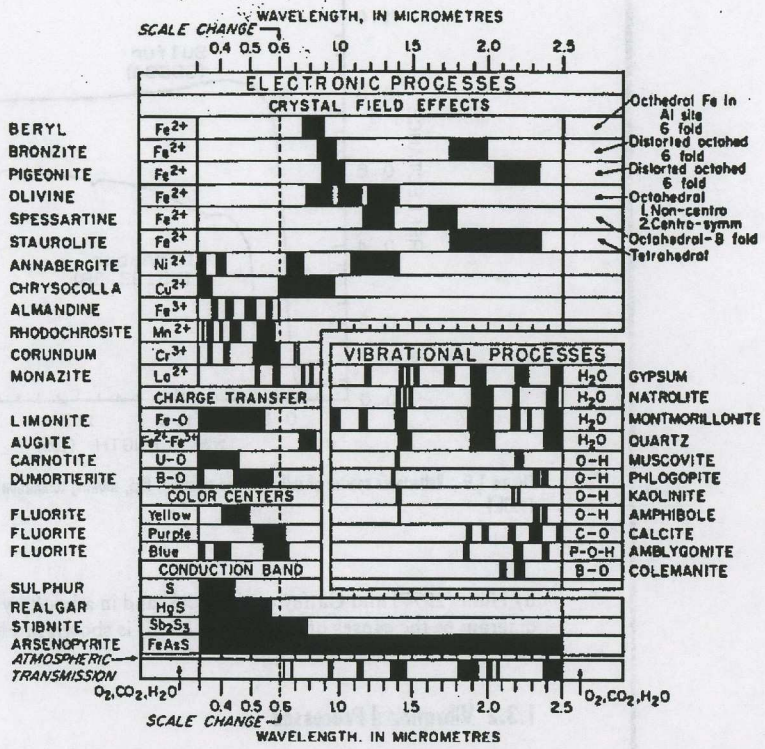

Figure 1.10 Spectral signature diagram. The widths of the black bars indicate the relative widths of absorption bands. (From Hunt, 1977.)

typically occur at very low energies (longer mid-infrared wavelengths), beyond about 20 μm.

Traditionally, the frequencies of fundamental vibrations are labeled with the Greek letter ν and a subscript (Herzberg, 1945). If a molecule has vibration fundamentals ν_1, ν_2, ν_3, it can have overtones at approximately $2\nu_1$, $3\nu_1$, $2\nu_2$ and combinations at approximately $\nu_1 + \nu_2$, $\nu_2 + \nu_3$, $\nu_1 + \nu_2 + \nu_3$, and so on. These examples used summations of modes, but subtractions are also possible (e.g. $\nu_1 + \nu_3 - \nu_2$). Each higher overtone or combination is typically 30 to 100 times weaker than the last. Consequently, the spectrum of a mineral can be quite complex. In reflectance spectroscopy, these weak absorptions can be measured easily and diagnostic information routinely gained from second and third overtones and combinations (e.g., Figures 1.5*b*, 1.6*b*, 1.7*b*, and 1.11 to 1.13).

Lattice modes are sometimes denoted by ν_T and ν_R and also couple with other

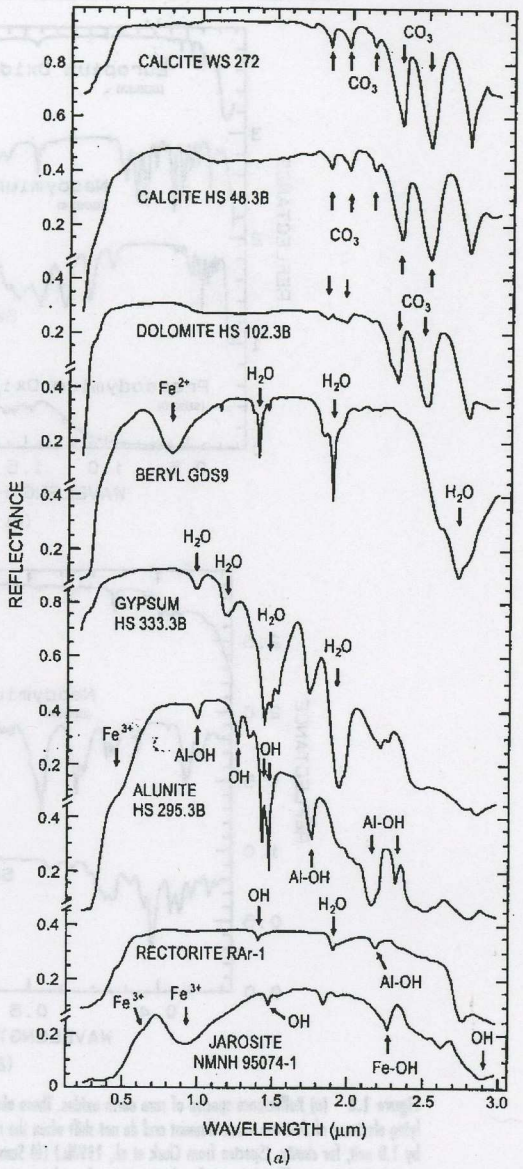

Figure 1.11 (*a*) Reflectance spectra of calcite, dolomite, beryl, gypsum, alunite, rectorite, and jarosite, showing vibrational bands due to OH, CO_3, and H_2O;

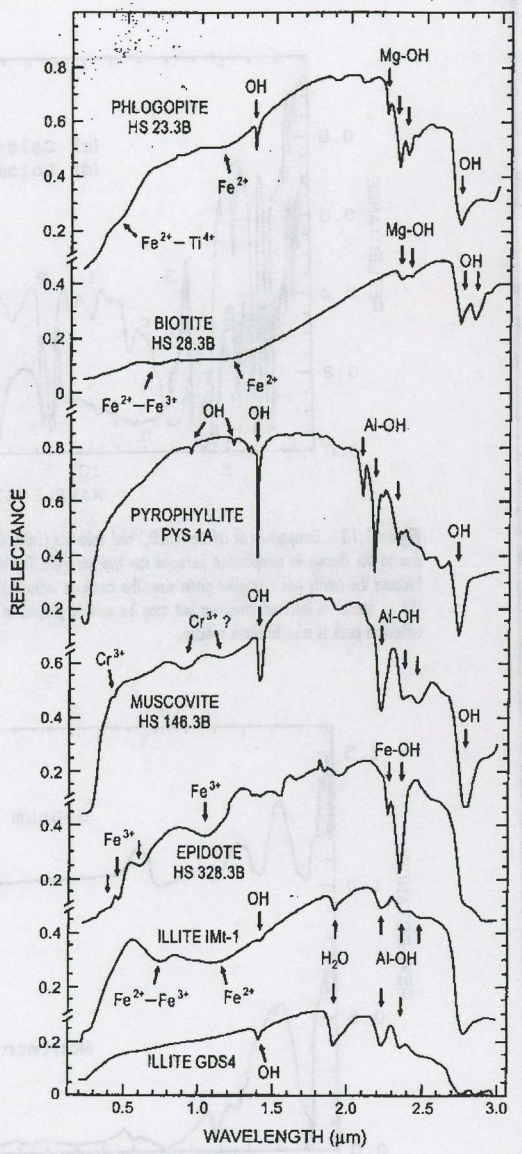

(*b*)

Figure 1.11 (*b*) reflectance spectra of phlogopite, biotite, pyrophyllite, muscovite, epidote, and illite showing vibrational bands due to OH and H_2O;

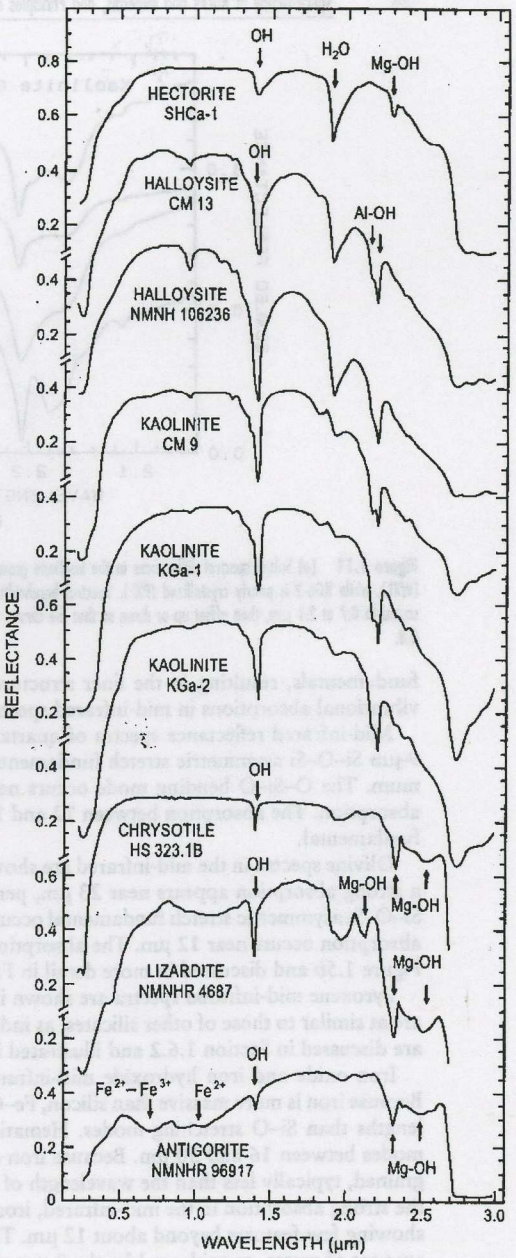

(*c*)

Figure 1.11 (*c*) Reflectance spectra of hectorite, halloysite, kaolinite, chrysotile, lizardite, and antigorite showing vibrational bands due to OH. (From Clark et al., 1990a.) Figure 1.19 shows an expanded view of the 1.4-μm region for chrysotile, lizardite, and antigorite.

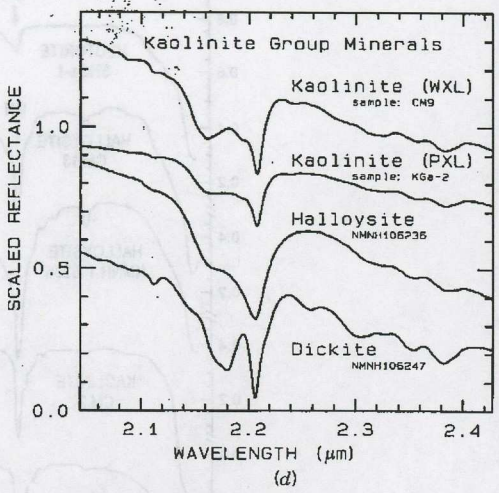

(*d*)

Figure 1.11 (*d*) Subtle spectral differences in the kaolinite group minerals near 2.2 μm. Kaolinite CM9 is well crystallized (WXL), while KGa-2 is poorly crystallized (PXL). Spectral bandwidth is 1.9 nm and sampling is 0.95 nm. Each spectrum was scaled to 0.7 at 2.1 μm, then offset up or down so that the curves do not overlap. Original reflectances were between 0.5 and 0.8.

fundamentals, resulting in the finer structure seen in some spectra. The causes of vibrational absorptions in mid-infrared spectra are summarized in Figure 1.14.

Mid-infrared reflectance spectra of quartz are shown in Figure 1.4*b*. The strong 9-μm Si–O–Si asymmetric stretch fundamental is obvious from the reflection maximum. The O–Si–O bending mode occurs near 25 μm and is the second strongest absorption. The absorption between 12 and 13 μm is the Si–O–Si symmetric stretch fundamental.

Olivine spectra in the mid-infrared are shown in Figure 1.5*b*. When Mg is present, a strong absorption appears near 23 μm, perhaps seen in the Fo 91 spectrum. The Si–O–Si asymmetric stretch fundamental occurs near 11 μm, and a weaker symmetric absorption occurs near 12 μm. The absorptions shift with composition as shown in Figure 1.5*b* and discussed in more detail in Farmer (1974, pp. 288–290).

Pyroxene mid-infrared spectra are shown in Figure 1.6*b*. The Si–O fundamentals are at similar to those of other silicates, as indicated in Figure 1.14. Grain size effects are discussed in Section 1.6.2 and illustrated in Figure 1.23.

Iron oxide and iron hydroxide mid-infrared spectra are shown in Figure 1.7*b*. Because iron is more massive than silicon, Fe–O fundamentals will be at longer wavelengths than Si–O stretching modes. Hematite, Fe_2O_3, has three strong stretching modes between 16 and 30 μm. Because iron oxides and hydroxides tend to be fine grained, typically less than the wavelength of mid-infrared photons, and because of the strong absorption in the mid-infrared, iron oxides tend to be dark in reflectance, showing few features beyond about 12 μm. The hematite in Figure 1.7*b* has a small amount of water, as evidenced by the 3-μm absorption, and a moderate amount of organics, as seen by the C–H stretch fundamental near 3.4 μm. The goethite, FeOOH, having hydroxyl, has a strong 3-μm absorption. The olivines (Figure 1.5) and py-

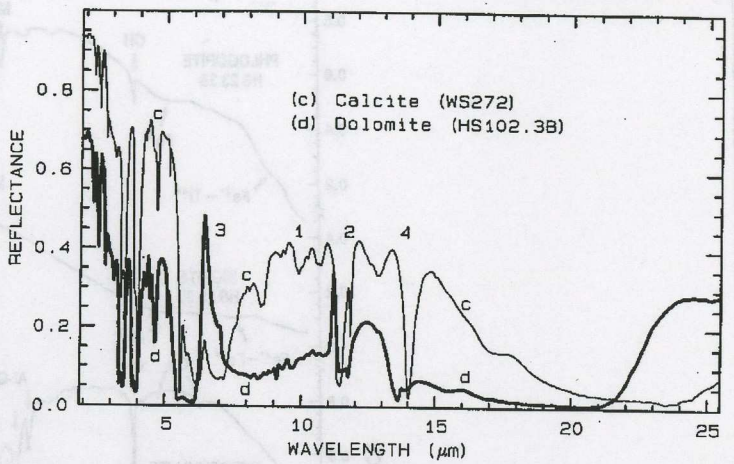

Figure 1.12 Comparison of calcite ($CaCO_3$) and dolomite ($CaMg(CO_3)_2$) spectra in the mid-infrared, showing small band shif due to the change in composition between the two minerals. The level change (calcite higher in reflectance than dolomite) because the calcite has a smaller grain size. The numbers indicate the fundamental stretching positions of ν_1, ν_2, ν_3, and ν The ν_1 stretch is infrared inactive but may be weakly present in carbonates. The ν_3 fundamental is so strong that only reflection peak is seen in these spectra.

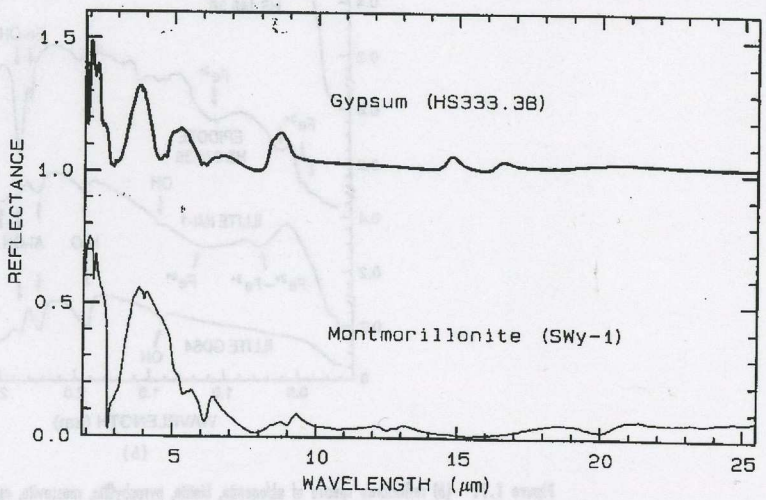

Figure 1.13 Mid-infrared spectra of gypsum, $CaSO_4 \cdot 2H_2O$ (top) and montmorillonite, $(Al,Mg)_8(Si_4O_{10})_3(OH)_{10} \cdot 12H_2O$ (bottom). The gypsum curve is offset upward 1.0 unit, for clarity. Both samples have very low reflectance because of the water content of the samples. Water is a strong infrared absorber. The montmorillonite also has a small grain size, which also tends to produce low mid-infrared reflectance because of the strong absorption in the mid-infrared.

roxenes (Figure 1.6) also show small amounts of water in the sample, as shown
the 3-μm absorptions in their spectra.

1.3.2.1 WATER AND HYDROXYL.

Water and OH (hydroxyl) produce particularly diagnostic absorptions in minera
The water molecule (H_2O) has $N = 3$, so there are $3N - 6 = 3$ fundamental vib
tions. In the isolated molecule (vapor phase) they occur at 2.738 μm (ν_1, symmet
OH stretch), 6.270 μm (ν_2, H–O–H bend), and 2.663 μm (ν_3, asymmetric O
stretch). In liquid water, the frequencies shift due to hydrogen bonding: ν_1
3.106μm, ν_2 = 6.079 μm, and ν_3 = 2.903 μm.

The overtones of water are seen in reflectance spectra of H_2O-bearing miner
(Figure 1.11). The first overtones of the OH stretches occur at about 1.4 μm and t
combinations of the H–O–H bend with the OH stretches are found near 1.9 μ
Thus a mineral whose spectrum has a 1.9-μm absorption band contains water (e.
hectorite and halloysite in Figure 1.11*c*), but a spectrum that has a 1.4-μm band b
no 1.9-μm band indicates that only hydroxyl is present (e.g., kaolinite in Figure 1.1
has only a small amount of water because of the weak 1.9-μm absorption but a lar
amount of OH). The hydroxyl ion has only one stretching mode, and its wavelen
position is dependent on the ion to which it is attached. In spectra of OH-beari
minerals, the absorption is typically near 2.7 to 2.8 μm but can occur anywhere
the range from about 2.67 to 3.45 μm (see, e.g., Clark et al., 1990, and referenc
therein). The OH commonly occurs in multiple crystallographic sites of a speci
mineral and is typically attached to metal ions. Thus there may be more than o
OH feature. The metal–OH bend occurs near 10 μm (usually superimposed on t
stronger Si–O fundamental in silicates). The combination metal–OH bend plus O
stretch occurs near 2.2 to 2.3 μm and is very diagnostic of mineralogy (see, e.
Clark et al., 1990a, and references therein).

1.3.2.2 CARBONATES.

Carbonates also show diagnostic vibrational absorption bands (Figures 1.11*a* a
1.12). The observed absorptions are due to the planar CO_3^{2-} ion. There are fo
vibrational modes in the free CO_3^{2-} ion: the symmetric stretch, ν_1: 1063 cm^{-1} (9.4
μm); the out-of-plane bend, ν_2: 879 cm^{-1} (11.4 μm); the asymmetric stretch, ν_3: 14
cm^{-1} (7.067 μm); and the in-plane bend, ν_4: 680 cm^{-1} (14.7 μm). The ν_1 band is n
infrared active in minerals. There are actually six modes in the CO_3^{2-} ion, but tw
are degenerate with the ν_3 and ν_4 modes. In carbonate minerals, the ν_3 and ν_4 ban
often appear as a doublet. The doubling has been explained in terms of the lifting
the degeneracy (see, e.g., White, 1974) due to mineral structure and anion site.

Combination and overtone bands of the CO_3 fundamentals occur in the nea
infrared. The two strongest are $\nu_1 + 2\nu_3$, at 2.50 to 2.55 μm (4000 to 3900 cm^{-1}
and $3\nu_3$ at 2.30 to 2.35 μm (4350 to 4250 cm^{-1}; e.g., Figure 1.11*a*). Three weak
bands occur near 2.12 to 2.16 μm ($\nu_1 + 2\nu_3 + \nu_4$ or $3\nu_1 + 2\nu_4$; 4720 to 4630 cm^{-1}
1.97 to 2.00 μm ($2\nu_1 + 2\nu_3$; 5080 to 5000 cm^{-1}), and 1.85 to 1.87 μm ($\nu_1 + 3\nu$
5400 to 5350 cm^{-1}; e.g., Figure 1.11*a*) (e.g., Hunt and Salisbury, 1971). The bar
positions in carbonates vary with composition (Hunt and Salisbury, 1971; Gaffe
1986, Gaffey et al., 1993). An example of such a band shift is seen in Figures 1.11
1.12, and in more detail in Figure 1.15, showing the shift in absorption position fro
calcite to dolomite.

Figure 1.14 Locations and causes of absorptions in mid-infrared spectra of silicates. (From Hunt, 1982.)

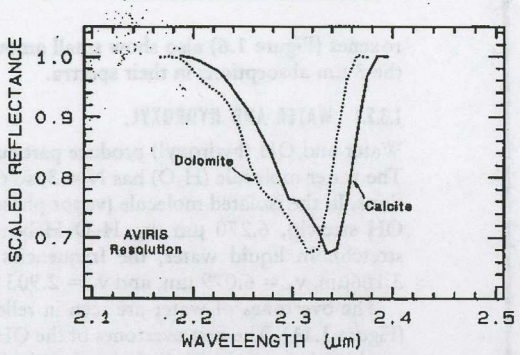

Figure 1.15 Comparison of calcite and dolomite continuum-removed features. The dolomite absorption occurs at a shorter wavelength than the calcite absorption.

1.3.2.3 OTHER MINERALS.

Phosphates, borates, arsenates, and vanadates also have diagnostic vibrational spectra. Space precludes inclusion of spectra here. See Hunt et al. (1972), and Clark et al. (1993b) for visual to near-infrared spectra. In general, the primary absorptions (e.g., P–O stretch) occurs at mid-infrared wavelengths. However, many of these minerals contain OH or H_2O and have absorptions in the near-infrared.

In the mid-infrared, minerals with H_2O, or those that are fine grained, like clays, have very low reflectance and show only weak spectral structure (e.g., Figure 1.13). Therefore, in emittance, spectral features will also be weak and thus difficult to detect. Grain size effects are discussed further below.

Typical spectra of minerals with vibrational bands are shown in Figures 1.4*b*, 1.5*b*, 1.6*b*, 1.7*b*, and 1.11. See Hunt and Salisbury (1970, 1971), Hunt et al. (1971a,b, 1972, 1973), Farmer (1974), Hunt (1979), Gaffey (1986, 1987), King and Clark (1989a), Clark et al. (1990a), Swayze and Clark (1990), Mustard (1992), Gaffey et al., 1993, and Salisbury (1993), and for more details. A summary of absorption band positions and causes is shown in Figures 1.10 and 1.14.

1.4 SPECTRA OF MISCELLANEOUS MINERALS AND MATERIALS

1.4.1 Organics

Organic materials are found all over the Earth and in the solar system. Organics can be important compounds in some environmental problems. The C–H stretch fundamental occurs near 3.4 μm (e.g., Figure 1.16*a*), the first overtone is near 1.7 μm, and a combination band is near 2.3 μm (Figure 1.16*b*). The combinations near 2.3 μm can sometimes be confused with OH and carbonate absorptions in minerals (e.g., Figure 1.11), especially at low spectral resolution. Further discussion and references appear in Chapter 3.

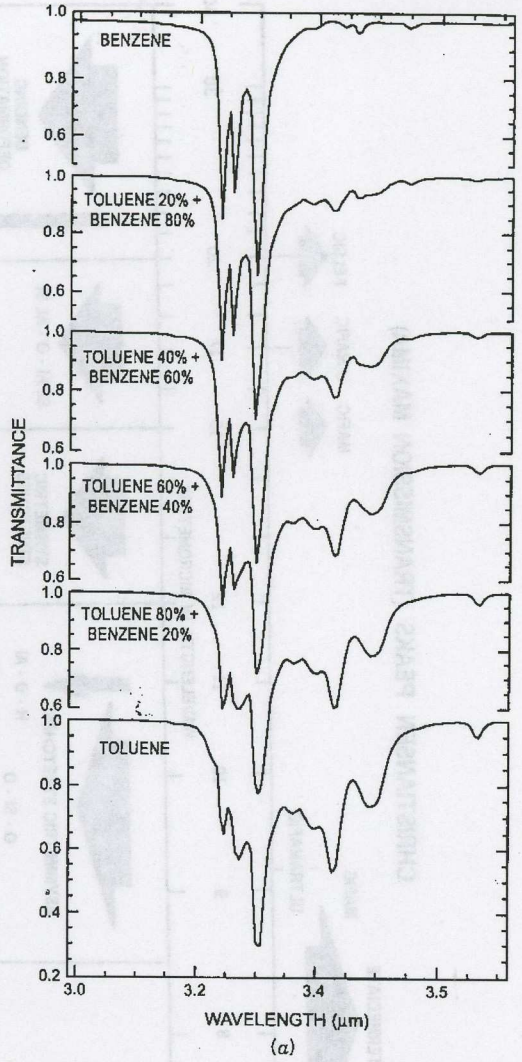

Figure 1.16 (*a*) Transmittance spectra of organics and mixtures showing the complex absorptions in the CH-stretch fundamen spectral region;

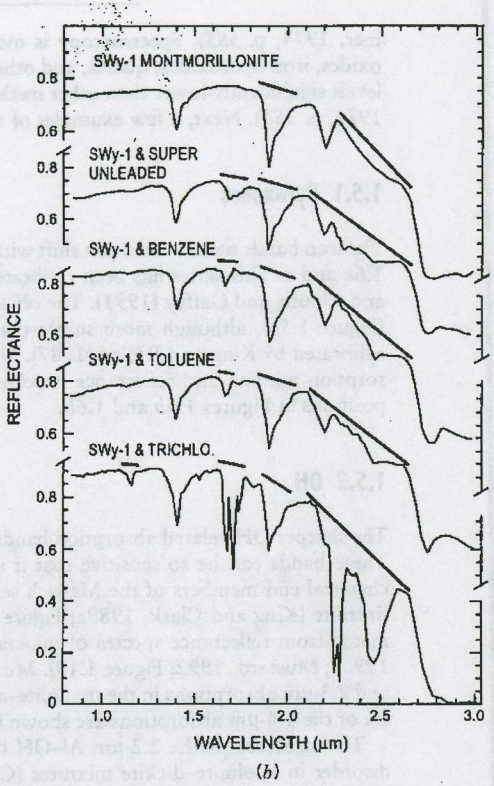

Figure 1.16 *(b)* reflectance spectra montmorillonite and montmorillonite mixed with super-unleaded gasoline, benzene, toluene, and trichlorethylene. Montmorillonite has an absorption feature at 2.2 μm, whereas the organics have a CH combination band near 2.3 μm. The first overtone of the CH stretch can be seen at 1.7 μm, and the second overtone near 1.15 μm. (From King and Clark, 1989b.)

1.4.2 Ices

Just as water in minerals shows diagnostic absorption bands, ice (crystalline H_2O), which is formally a mineral, also shows strong absorption bands. In the planetary literature it is referred to as water ice so as not to confuse it with other ices. Spectra of solid H_2O, CO_2, and CH_4 are shown in Figure 1.17. The spectral features in Figure 1.17 are all due to vibrational combinations and overtones, whose fundamentals have previously been discussed in general. Note that the H_2O spectra show broad absorptions compared to the others. The reason is that while ice is normally a hexagonal structure, the hydrogen bonds are orientationally disordered (e.g., Hobbs, 1974), and the disorder broadens the absorptions. There are many ices in the solar system (see, e.g., reviews by Cruikshank et al., 1985 and Clark et al., 1986,).

Ice, being ubiquitous in the solar system is found mixed with other minerals, on

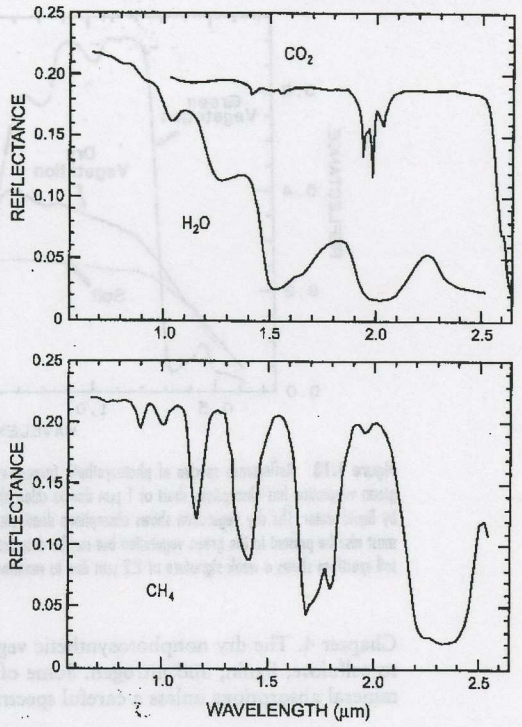

Figure 1.17 Reflectance spectra of solid carbon dioxide (CO_2), methane (CH_4), and water (H_2O). (From Clark et al., 19

the Earth, as well as elsewhere in the solar system (e.g., Clark et al., 1986). T spectral properties of ice and ice–mineral mixtures have been studied by Cla (1981a,b), Clark and Lucey (1984), Lucey and Clark (1985), and references there

1.4.3 Vegetation

Spectra of vegetation come in two general forms: green and wet (photosynthetic) a dry nonphotosynthetic, but there is a seemingly continuous range between these tv end members. The spectra of these two forms are compared to a soil spectrum Figure 1.18. Because all plants are made of the same basic components, their spect appear generally similar. However, in the spectral analysis section we will see met ods for distinguishing subtle spectral details. The near-infrared spectra of green ve etation are dominated by liquid-water vibrational absorptions. The water bands a shifted to slightly shorter wavelengths than in liquid water, due to hydrogen bondin The absorption in the visible is due to chlorophyll and is discussed in more detail

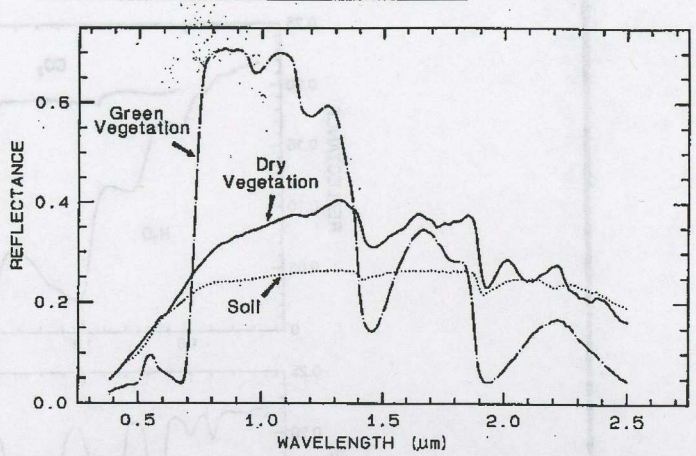

Figure 1.18 Reflectance spectra of photosynthetic (green) vegetation, nonphotosynthetic (dry) vegetation, and a soil. The green vegetation has absorptions short of 1 μm due to chlorophyll. Those at wavelengths greater than 0.9 μm are dominated by liquid water. The dry vegetation shows absorptions dominated by cellulose, but also lignin and nitrogen. These absorptions must also be present in the green vegetation but can be detected only weakly in the presence of the stronger water bands. The soil spectrum shows a weak signature at 2.2 μm due to montmorillonite.

Chapter 4. The dry nonphotosynthetic vegetation spectrum shows absorptions due to cellulose, lignin, and nitrogen. Some of these absorptions can be confused with mineral absorptions unless a careful spectral analysis is done.

1.5 SENSITIVITY OF ABSORPTION BANDS TO CRYSTAL STRUCTURE AND CHEMISTRY

Reflectance spectroscopy shows a wealth of information about mineralogy. Why, then, is spectroscopy not used more widely? In many cases spectroscopy is very sensitive to subtle changes in crystal structure or chemistry. This has resulted in confusion in the past over cause and effect. More recently, this sensitivity has been recognized as a powerful means of studying the structure and composition of minerals. Additional problems occur with reflectance spectra due to scattering and are discussed below.

Because spectroscopy is sensitive to so many processes, the spectra can be very complex and there is still much to learn. However, it is because of this sensitivity that spectroscopy has great potential as a diagnostic tool. In fact, for some materials, spectroscopy is an excellent tool not only for detecting certain chemistries, but also at abundance levels unmatched by other tools. For example, each layer of a layered silicate absorbs radiation almost independently from its neighbors. The absorption of photons does not depend on the longer-range crystallographic order as is required to give distinctive x-ray diffraction patterns. Thus, many processes (e.g., clay dehydroxylation) are detectable with spectroscopy before other methods (see, e.g., Farmer, 1974, p. 355). Spectroscopy is more sensitive to the presence of clays, i oxides, iron hydroxides, quartz, and other minerals with strong absorption band levels significantly lower than other methods, such as x-ray diffraction (e.g., Farm 1974, p. 355). Next, a few examples of the possibilities are shown.

1.5.1 Pyroxenes

The iron bands near 1 and 2 μm shift with pyroxene composition as shown in Fig 1.6*a* and *c*. This series has been calibrated by Adams (1975), Cloutis et al. (198 and Cloutis and Gaffey (1991). The olivine 1-μm band also shifts with composit (Figure 1.5*a*), although more subtly than with pyroxenes, and the shift has b calibrated by King and Ridley (1987). Note also the shifts, seen as positions of sorption minima and reflectance maxima, in the mid-infrared with different co positions in Figures 1.5*b* and 1.6*b*.

1.5.2 OH

The sharper OH-related absorption bands allow smaller band shifts to be measur These bands can be so sensitive that it is possible to distinguish between the i chemical end members of the Mg-rich serpentine group, chrysotile, antigorite, a lizardite (King and Clark, 1989a; Figure 1.19). The Fe:Fe + Mg ratio can be es mated from reflectance spectra of minerals with brucitelike structure (Clark et a 1990a, Mustard, 1992; Figure 1.19). Mustard (1992) calibrated changes in the 1 and 2.3-μm absorptions in the tremolite–actinolite solid solution series; sample sp tra of the 1.4-μm absorptions are shown in Figure 1.19.

The structure of the 2.2-μm Al–OH band has been shown to be diagnostic disorder in kaolinite–dickite mixtures (Crowley and Vergo, 1988) and the deg of kaolinite crystallinity (Clark et al., 1990a), which is illustrated in Figure 1.1 and *d*.

The strong and sharp OH features have proven particularly diagnostic of cl mineralogy, perhaps better than with x-ray diffraction (XRD) analysis (like a method, spectroscopy has advantages in some areas, and XRD in others). For e ample, it appears easy to distinguish kaolinite from halloysite with spectroscopy (e. Clark et al., 1990a), as shown in Figures 1.11*c* and *d*. Montmorillonite is eas distinguished from illite or muscovite (e.g., Clark et al., 1990a), whereas XRD an ysis combines them into the general term *smectites*.

1.5.3 Al in Muscovite

More recently, subtle shifts have been found in muscovite series with aluminu composition (e.g., Post and Noble, 1993; Duke, 1994; Swayze, 1997). As elemen substitute for aluminum in the crystal structure, the crystal becomes slightly distort relative to no substitutions. This causes slight changes in Al–O–H bond lengths a thus shifts absorption band position. Sample shifts with composition are shown Figure 1.20. In this case the shift of the 2.2-μm absorption appears continuous wi

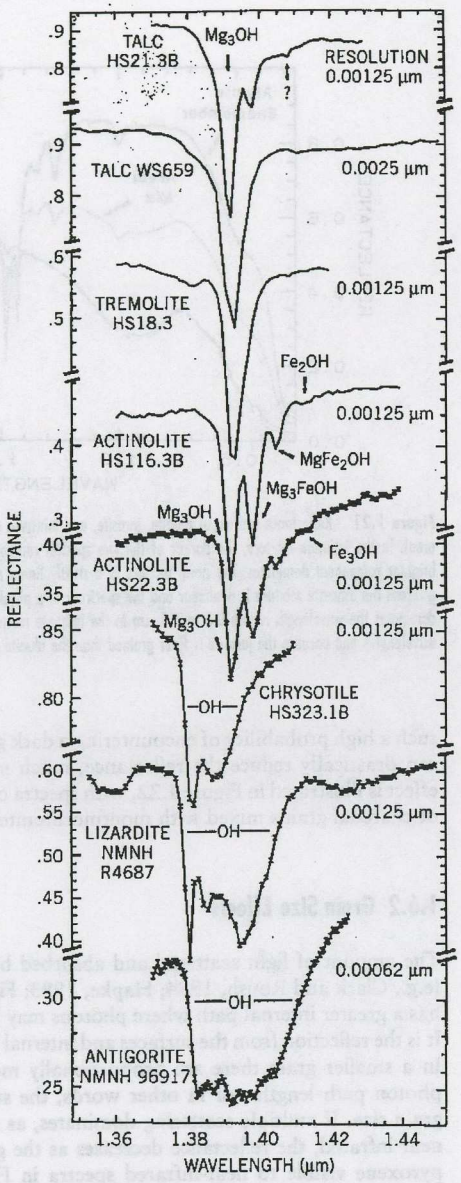

Figure 1.19 High-spectral-resolution reflectance spectra of the first overtone of OH in talc, tremolite, actinolite, crysotile, lizardite, and antigorite. The three sharp absorption bands in talc, tremolite, and actinolite are caused by Mg and Fe ions associated with the hydroxyls, causing small band shifts. The Fe:Fe + Mg ratio can be estimated. In chrysotile, lizardite, and antigorite, the absorptions change with small structural differences, even though the composition is constant. (From Clark et al., 1990a.)

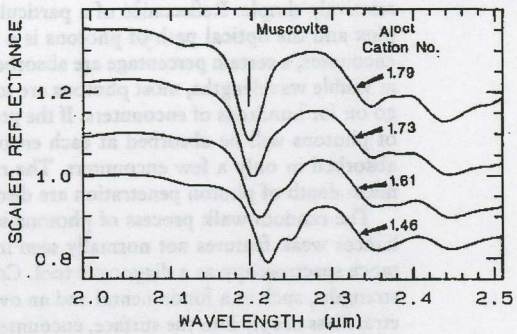

Figure 1.20 Reflectance spectra of muscovite, showing band shifts due to changing aluminum composition. (From Swa 1997.)

composition, compared to the growth of specific absorptions as in the tremolit actinolite series shown in Figure 1.19. It is likely that all muscovite-group miner show similar behavior, and illites may also.

1.5.4 Discussion

Reflectance spectroscopy can be used without sample preparation, and it is nond structive. This makes mapping of exposed minerals from aircraft possible, includi detailed clay mineralogy (e.g., Clark et al., 1993a). Visual and near-infrared spe troscopy, on the other hand, is insensitive to some minerals that do not have a sorptions in this wavelength region. For example, quartz has no diagnostic spectr features in the visible and near-infrared; in fact, it is used as optical components many telescopes and prisms. Quartz must be detected at its fundamental Si–O stretc ing region near 10 μm, as shown in Figure 1.4*b*.

Now that we have explored the causes of absorption features in minerals, explore how those features get modified.

1.6 SCATTERING PROCESS

Scattering is the process that makes reflectance spectroscopy possible. Photons ent a surface, are scattered one or more times, and while some are absorbed, others a scattered from the surface, so we may see and detect them. Scattering can also thought of as scrambling information. The information is made more complex, a because scattering is a nonlinear process, recovery of quantitative information more difficult.

Consider the simple Beer's law in equation (1.2). In transmission, light pass through a slab of material. There is little or no scattering (none in the ideal case; b there are always internal reflections from the surfaces of the medium). Analysis

relatively simple. Reflectance of a particulate surface, however, is much more complex and the optical path of photons is a random walk. At each grain the photons encounter, a certain percentage are absorbed. If the grain is bright, like a quartz grain at visible wavelengths, most photons are scattered and the random walk process can go on for hundreds of encounters. If the grains are dark, like magnetite, the majority of photons will be absorbed at each encounter and essentially all photons will be absorbed in only a few encounters. The random walk process, scattering, and the mean depth of photon penetration are discussed in Clark and Roush (1984).

The random walk process of photons scattering in a particulate surface also enhances weak features not normally seen in transmittance, further increasing reflectance spectroscopy as a diagnostic tool. Consider two absorption bands of different strengths, such as a fundamental and an overtone. The stronger absorption will penetrate less deeply into the surface, encountering fewer grains because the photons are absorbed. At the wavelengths of the weaker absorption, fewer photons are absorbed with each encounter with a grain, so the random walk process goes further, increasing the average photon path length. The greater path length will result in more absorption, thus strengthening the weak absorption in a reflectance spectrum.

1.6.1 Mixtures

The real world (and for that matter, the universe) is a complex mixture of materials, at just about any scale at which we view it. In general, there are four types of mixtures:

1. *Linear mixture.* The materials in the field of view are optically separated, so there is no multiple scattering between components. The combined signal is simply the sum of the fractional area times the spectrum of each component. This is also called *areal mixture.*
2. *Intimate mixture.* An intimate mixture occurs when different materials are in intimate contact in a scattering surface, such as the mineral grains in a soil or rock. Depending on the optical properties of each component, the resulting signal is a highly nonlinear combination of the end-member spectra.
3. *Coatings.* Coatings occur when one material coats another. Each coating is a scattering–transmitting layer whose optical thickness varies with material properties and wavelength.
4. *Molecular mixtures.* Molecular mixtures occur on a molecular level, such as two liquids or a liquid and a solid mixed together. Examples: water adsorbed onto a mineral; gasoline spilled onto a soil. The close contact of the mixture components can cause band shifts in the adsorbate, such as the interlayer water in montmorillonite or the water in plants.

An example mixture comparison is shown in Figure 1.21 for alunite and jarosite. Note in the intimate mixture how the jarosite dominates in the region 0.4 to 1.3 μm. The reason is because in an intimate mixture, the darker material dominates because photons are absorbed when they encounter a dark grain. In the areal mixture, the brighter material dominates.

In a mixture of light and dark grains (e.g., quartz and magnetite) the photons have

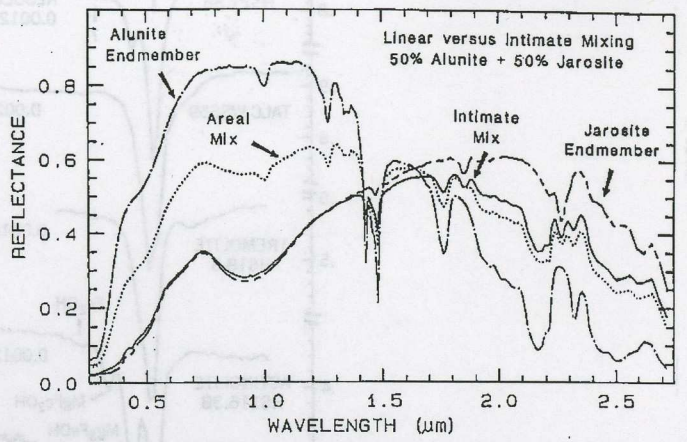

Figure 1.21 Reflectance spectra of alunite, jarosite, and mixtures of the two. Two mixtures types are shown: intimate areal. In the intimate mixture, the darker of the two spectral components tends to dominate, and in the areal mixture, brighter component dominates. The areal mixture is a strictly linear combination and was computed from the end memb whereas the intimate mixture is nonlinear and the spectrum of a physical mixture was measured in the laboratory. The jaro dominates the wavelength region 0.3 to 1.4 μm in the intimate mixture because of the strong absorption in jarosite at th wavelengths and because the jarosite is finer grained than the alunite and tends to coat the larger alunite grains.

such a high probability of encountering a dark grain that a few percent of dark grai can drastically reduce the reflectance, much more than their weight fraction. T effect is illustrated in Figure 1.22, with spectra of samples having various proportio of charcoal grains mixed with montmorillonite.

1.6.2 Grain Size Effects

The amount of light scattered and absorbed by a grain is dependent on grain si (e.g., Clark and Roush, 1984; Hapke, 1993; Figures 1.23 and 1.24). A larger gra has a greater internal path where photons may be absorbed according to Beer's la It is the reflection from the surfaces and internal imperfections that control scatterin In a smaller grain there are proportionally more surface reflections than intern photon path lengths, or in other words, the surface/volume ratio is a function grain size. If multiple scattering dominates, as is usually the case in the visible ar near-infrared, the reflectance decreases as the grain size increases, as shown in th pyroxene visible to near-infrared spectra in Figure 1.23*a*. However, in the mi infrared, where absorption coefficients are much higher and the index of refracti varies strongly at the Christensen frequencies, the first surface reflection is a larg or even dominant component of the scattered signal. In these cases the grain si effects are much more complex, even reversing trends commonly seen at short wavelengths (e.g., Figure 1.23*b*).

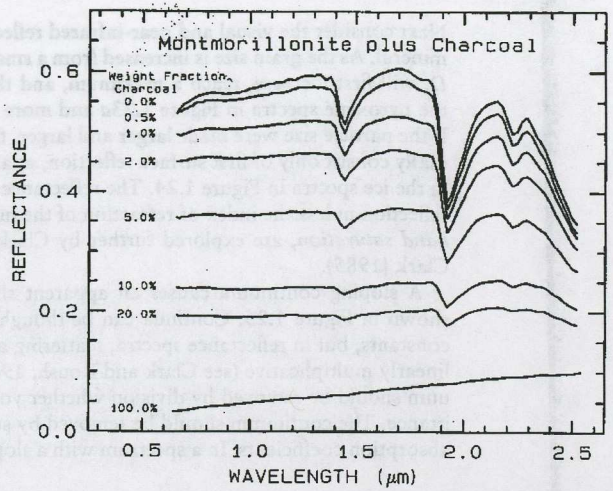

Figure 1.22 Reflectance spectra of intimate mixtures of montmorillonite and charcoal illustrates the nonlinear aspect of reflectance spectra of mixtures. The darkest substance dominates at a given wavelength. (From Clark, 1983.)

1.6.3 Continuum and Band Depth

Absorptions in a spectrum have two components: continuum and individual features. The continuum is the background absorption onto which other absorption features are superimposed (see, e.g., Clark and Roush, 1984). It may be due to the wing of a larger absorption feature. For example, in the pyroxene spectra in Figure 1.23*a*, the weak feature at 2.3 μm is due to a trace amount of tremolite in the sample and the absorption is superimposed on the broader 2-μm pyroxene band. The broader pyroxene absorption is the continuum to the narrow 2.3-μm feature. The pyroxene 1.0-μm band is superimposed on the wing of a stronger absorption centered in the ultraviolet.

The depth of an absorption band, D, is usually defined relative to the continuum, R_c:

$$D = 1 - \frac{R_b}{R_c} \tag{1.6}$$

where R_b is the reflectance at the band bottom and R_c is the reflectance of the continuum at the same wavelength as R_b (Clark and Roush, 1984).

The depth of an absorption is related to the abundance of the absorber and the grain size of the material. Consider a particulate surface with two minerals, one whose spectrum has an absorption band. As the abundance of the second mineral is increased, the band depth, D, of the absorption in the first mineral will decrease.

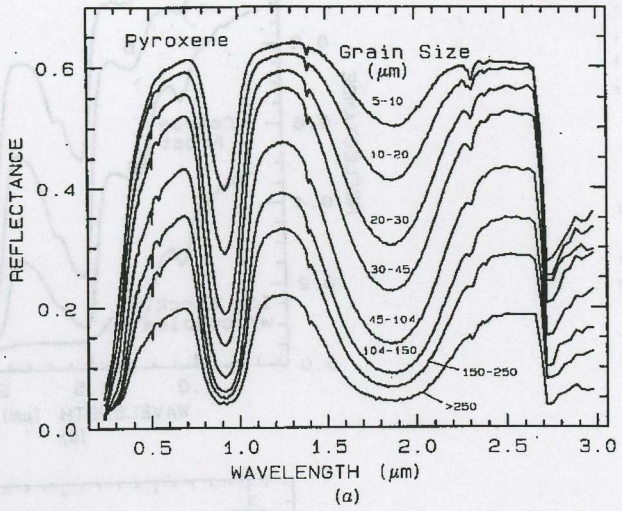

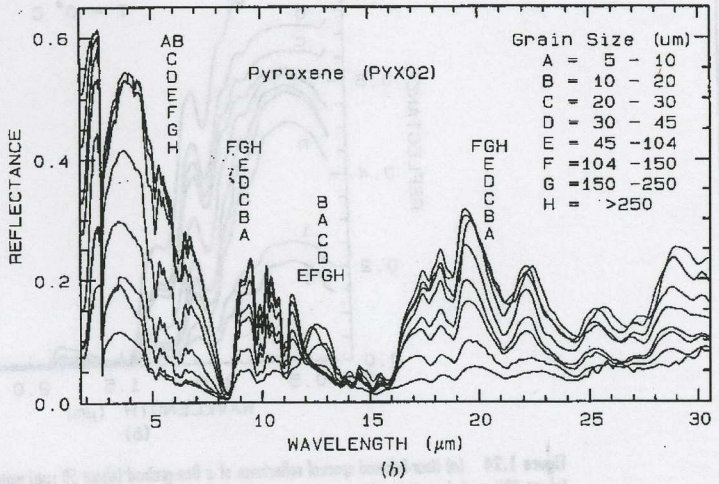

Figure 1.23 (*a*) Reflectance spectra of pyroxene as a function of grain size. As the grain size becomes larger, more li absorbed and the reflectance drops. (From Clark et al., 1993b.) (*b*) Same series as in part (*a*), but for the mid-infrared position of letter identifiers indicates the relative position of the spectra at the various wavelengths. Note the reversal i trends at some wavelengths and not others. Grain size effects on the shapes of spectral features in the mid-infrared ca quite large.

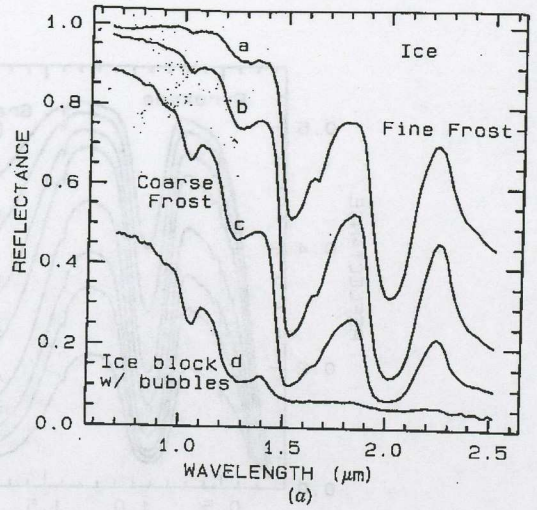

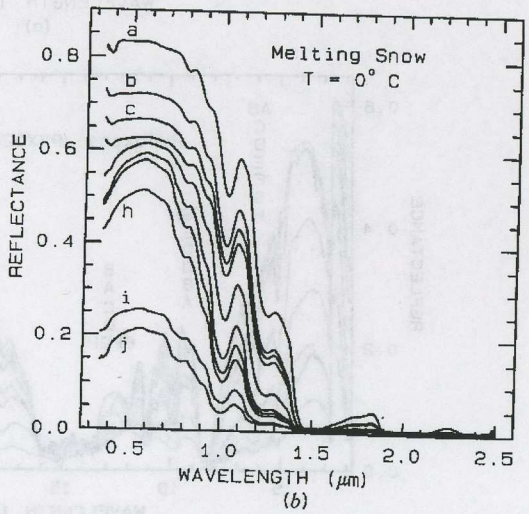

Figure 1.24 *(a)* Near-infrared spectral reflectance of a fine-grained (about 50 μm) water frost (curve a), medium-grained (about 200 μm) frost (curve b), coarse-grained (400 to 2000 μm) frost (curve c), and an ice block containing abundant microbubbles (curve d). The larger the effective grain size, the greater the mean photon path that photons travel in the ice, and the deeper the absorptions become. Curve d is very low in reflectance because of the large path length in ice. The ice temperatures for these spectra are 112 to 140 K. (From Clark et al., 1986.) *(b)* Series of reflectance spectra of melting snow. Curve a is at 0°C and has only a small amount of liquid water, whereas the lowest spectrum (curve j) is of a puddle of about 3 cm of water on top of the snow. Note in the top spectrum that there is no 1.65-μm band as in the ice spectra in part *(a)* because of the higher temperature. The 1.65-μm feature is temperature dependent and decreases in strength with increasing temperature (see Clark, 1981a, and references therein). Note the increasing absorption at about 0.75 μm and in the short side of the 1-μm ice band as more liquid water forms. The liquid water becomes spectrally detectable at about spectrum e, when the UV absorption increases. (Spectra from Clark et al., submitted).

Next consider the visual and near-infrared reflectance spectrum of a pure powde
mineral. As the grain size is increased from a small value, the absorption-band dep
D, will first increase, reach a maximum, and then decrease. This can be seen w
the pyroxene spectra in Figure 1.23*a* and more so in the ice spectra in Figure 1.
If the particle size were made larger and larger, the reflectance spectrum would ev
tually consist only of first surface reflection, as at most wavelengths beyond 1.45
in the ice spectra in Figure 1.24. The reflectance can never go to zero because of t
reflection unless the index of refraction of the material is 1.0. These concepts, cal
band saturation, are explored further by Clark and Lucey (1984) and Lucey a
Clark (1985).

A sloping continuum causes an apparent shift in the reflectance minimum,
shown in Figure 1.25. Continua can be thought of as an additive effect of opti
constants, but in reflectance spectra, scattering and Beer's law make the effects n
linearly multiplicative (see Clark and Roush, 1984, for more details). So the cont
uum should be removed by division whether you are working in reflectance or e
ittance. The continuum should be removed by subtraction only when working w
absorption coefficients. In a spectrum with a sloping continuum, correction remo

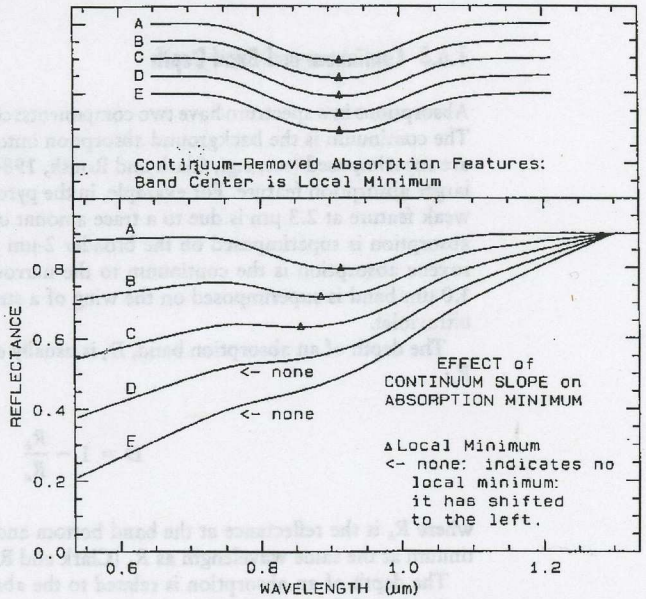

Figure 1.25 Continua and continuum removal. In the lower set of curves, the local minimum in the curve shifts to sho
wavelengths with increasing slope. Removal of the continuum by division isolates the spectral features so they may be compa
(top). The top set of curves are offset for clarity. In the continuum-removed spectra, we can see that there is no real shi
the absorption-band center.

the effect of shifts in the local reflectance minimum (Figure 1.25). Note your perception of spectrum E versus A in Figure 1.25. The spectral features do not appear to be the same, but if you remove the continuum, it is obvious that they are the same (Figure 1.25, top).

1.6.4 Continuum-Removed Spectral Feature Comparison

The continuum-removal process isolates spectral features and puts them on a level playing field so they may be intercompared. Continuum removal and feature comparison is the key to successful spectral identification. For example, compare the spectra of calcite ($CaCO_3$) and dolomite ($CaMg(CO_3)_2$) in Figure 1.11*a*. If we isolate the spectral features, remove the continuum, and scale the band depth (or band area) to be equal, we can see subtle band shifts and shapes (Figure 1.15). Now compare a harder case: halloysite and kaolinite (Figure 1.11*c*). You might note that halloysite has a different absorption feature at 1.9 μm. However, if you were obtaining the spectrum through the Earth's atmosphere, you would have virtually no data in that wavelength region because atmospheric water absorbs too much of the signal. The diagnostic feature is the 2.2-μm band. The continua-removed 2.2-μm features for halloysite and kaolinite are shown in Figure 1.26, where we can see significant differences between the spectra of the two minerals.

One of the most challenging spectral features to distinguish between are those in spectra of various plant species. Figure 1.27*a* shows four plant spectra (the spectra are offset for clarity). The overall shapes are quite similar. If we remove the continuum according to Figure 1.27*b*, we see the detailed chlorophyll absorption spectral variations for these as well as other plants in Figure 1.27*c*. Shape-matching algorithms, such as that presented in Clark et al. (1990b), can distinguish between these spectra and compare them accurately to spectral libraries (see, e.g., Clark et al., 1993b; Chapter 5).

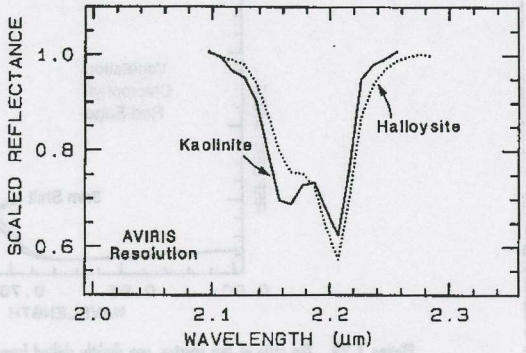

Figure 1.26 Comparison of kaolinite and halloysite spectral features. Both mineral spectra have the same band position at 2.2 μm. However, the kaolinite spectrum shows a stronger feature at 2.16 μm than in the halloysite spectrum.

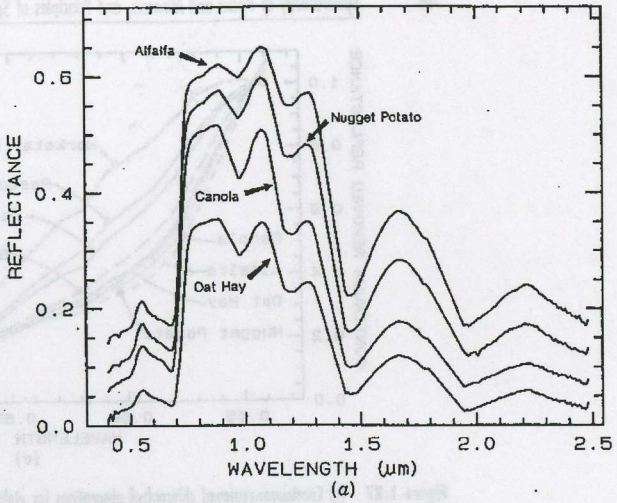

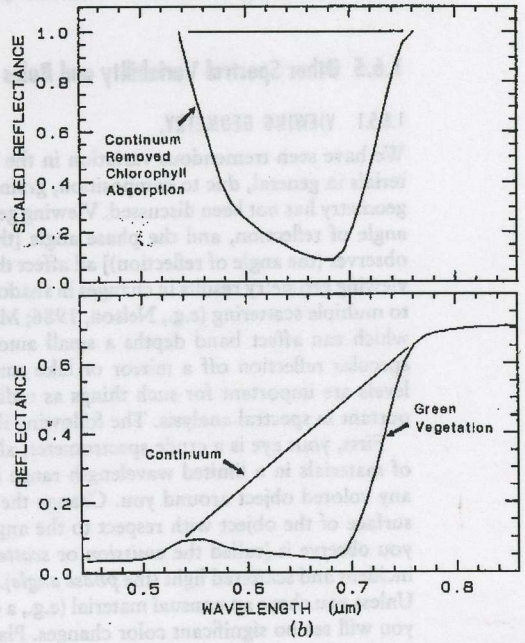

Figure 1.27 (*a*) Reflectance spectra for four types of vegetation. Each curve is offset by 0.05 reflectance unit from the below. (From Clark et al., 1995, submitted.) (*b*) Continuum-removal example for a chlorophyll absorption in vegetation.

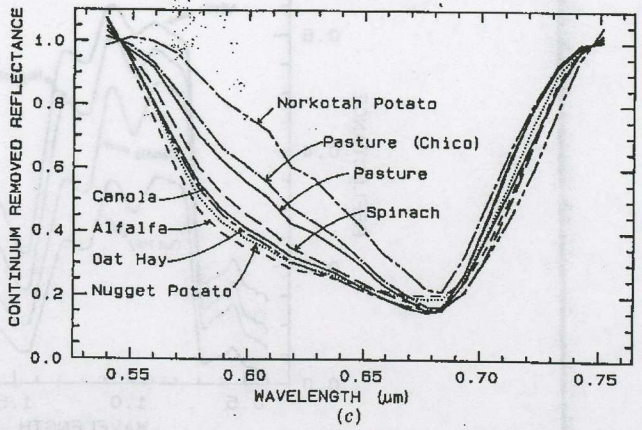

Figure 1.27 (c) Continuum-removed chlorophyll absorptions for eight vegetation types [including the four from part (a)], showing that the continuum-removed features can show subtle spectral differences. (From Clark et al., 1995, submitted.)

1.6.5 Other Spectral Variability and Rules

1.6.5.1 VIEWING GEOMETRY.

We have seen tremendous variation in the spectral properties of minerals and materials in general, due to composition, grain size, and mixture types. So far, viewing geometry has not been discussed. Viewing geometry, including the angle of incidence, angle of reflection, and the phase angle [the angle between the incident light and observer (the angle of reflection)] all affect the intensity of light received. Varying the viewing geometry results in changes in shadowing and the proportions of first surface to multiple scattering (e.g., Nelson, 1986; Mustard and Pieters, 1989; Hapke, 1993), which can affect band depths a small amount except in rare cases (e.g., extreme specular reflection off a mirror or lake surface). Whereas measuring precise light levels are important for such things as radiation balance studies, they are less important in spectral analysis. The following illustrates why.

First, your eye is a crude spectrometer, able to distinguish the spectral properties of materials in a limited wavelength range by the way we interpret color. Pick up any colored object around you. Change the orientation of the local normal on the surface of the object with respect to the angle of incident light, the angle at which you observe it (called the *emission* or *scattering angle*), and the angle between the incident and scattered light (the *phase angle*). As you do this, note any color changes. Unless you chose an unusual material (e.g., a diffraction grating or very shiny object), you will see no significant color changes. Plant leaves appear green from any angle, a pile of hematite appears red from any angle. This tells you that the spectral features do not change much with viewing geometry. Your eye–brain combination normalizes intensity variations so that you see the same color, regardless of the actual brightness of the object (the amount of light falling on the surface). The continuum removal does a similar but more sophisticated normalization. The band depth, shape, and position are basically constant with viewing geometry. Band depth will change only

with the proportion of specular reflection added to the reflected light. For surfa (and at wavelengths) where multiple scattering dominates, that change in band de is minimized.

1.6.5.2 RATIOING SPECTRA.

Ratioing two spectra with spectral features can cause spurious features in the ra (e.g., Clark and King, 1987). However, this ratio can be used to advantage. Consi two spectra, with an absorption edge, such as conduction bands in cinnabar (Fig 1.9), sulfur, or the chlorophyll-absorption edge in plants at 0.7 μm. If one spectr is shifted relative to the other and then the two ratioed, the resulting ratio ha residual feature that looks like either an absorption or emission feature (depend on the direction of the shift and which spectrum is the numerator and which is denominator). A sample residual caused by such shifts is shown in Figure 1.28. T effect has recently been used to determine subtle shifts in the chlorophyll absorpt edge in plants (Clark et al., 1995, 1996). The intensity of the feature in the reflecta

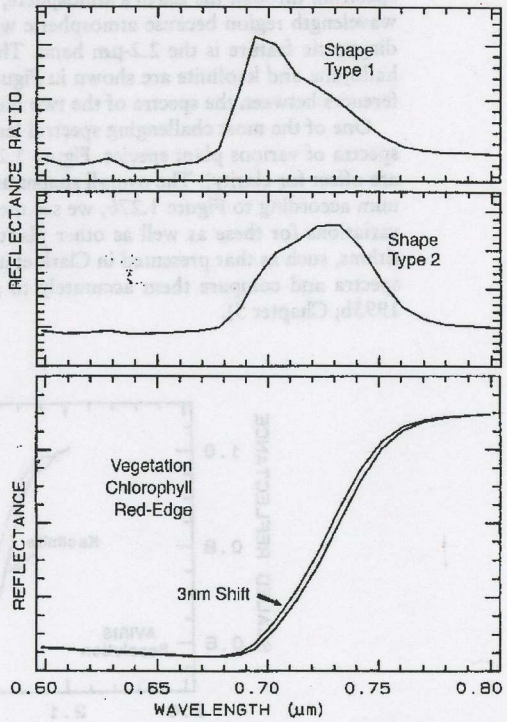

Figure 1.28 The ratio of two spectra, one slightly shifted from the other, results in a spectral feature. The two shap this example are from different chlorophyll bands. Shifts as small as 0.01 times the full width at half maximum of spectrometer system produce 1% features in strong chlorophyll absorptions. The shape, type 1 profile, is from the shifted sp shown at the bottom of the figure, while the shape, type 2, is from shallower chlorophyll absorptions. (From Clark et submitted.)

ratio is proportional to the amount of shift between the two spectra, and the shape of the ratio does not change if the shifts are small. Clark et al. (1995, 1998) showed that chlorophyll-edge shifts as small as 0.01 times the bandwidth of the spectrometer can be detected. Thus for the AVIRIS system with 10-nm bandpass and sampling, shifts of 0.1 nm can readily be detected. Such sensitivity indicates that the wavelength stability of a spectrometer must be very good for such analyses.

1.6.5.3 IRON OXIDE, HYDROXIDE, AND SULFATE COMPLEXITY.

Iron oxides, hydroxides, and sulfates are a special case for remote sensing because they are so ubiquitous. Further, because of the strength of the iron absorptions in the ultraviolet to about 1 μm, at least one if not all are saturated in reflectance. Several hematite reflectance spectra at different grain sizes are shown in Figure 1.29*a*. Nanocrystalline hematite (Morris et al., 1985) has such a fine grain size, ≤25 nm, that the grain surface boundary modifies the electronic transitions, changing and weakening them. The iron absorption at 0.9 μm is reduced in depth, the 0.65-μm band is absent, and the ultraviolet absorption is weak. Absorptions in transmittance, as in the thin-film case, are $\sqrt{2}$ times narrower in width (see Clark and Roush, 1984). Larger grain sizes show increased saturation of the 0.9-μm absorption, broadening and shifting the apparent reflectance minimum to longer wavelengths. The 0.9-μm absorption also shifts position with elements substituted for iron (see, e.g., Morris et al., 1985, and references therein). Continuum removal and scaling the hematite absorption to similar depth show the wide variety of band shapes and positions that can be found in nature (Figure 1.29*b*).

There are a whole suite of iron oxides, iron hydroxides, iron sulfates, and so on, some only now being discovered, and many amorphous phases, all with similar electronic absorption bands in the visible and near-infrared. A few examples are shown in Figure 1.30*a*. Note that hematite has a narrower absorption at a slightly shorter wavelength than goethite. However, a coarse-grained hematite has a broader absorption, approaching the position and width of a fine-grained goethite (or a thin-film goethite).

Jarosite has a narrow absorption near 0.43 μm, but it sometimes appears weak because of the saturated UV absorption. Jarosite, an iron sulfate, has a diagnostic absorption at 2.27 μm due to a combination OH stretch and Fe–OH bend. However, this feature is weaker than the electronic absorptions in the visible and is often masked by clay or alunite (jarosite often occurs in hydrothermal deposits with alunite). The features near 1.475 μm and 1.8 μm are OH related and are commonly seen in sulfate spectra.

Ferrihydrite is an amorphous iron oxide, and its spectrum appears very similar to the orange precipitate, an amorphous iron hydroxide, obtained downstream from the Summitville, Colorado mine (King et al., 1995). However, if we remove the continuum and compare the positions and shapes of the bands (Figure 1.30*b*), we see that they are indeed different.

As discussed above, there are many iron-bearing minerals and amorphous materials with similar but distinct absorption bands. How many can be distinguished with reflectance spectroscopy is still a matter of research. An even harder question to answer is how many can be distinguished and not be confused with mixtures of other iron-bearing materials. Detailed spectral analysis, including continuum removal to isolate absorption features, can certainly improve the success of distinguishing them.

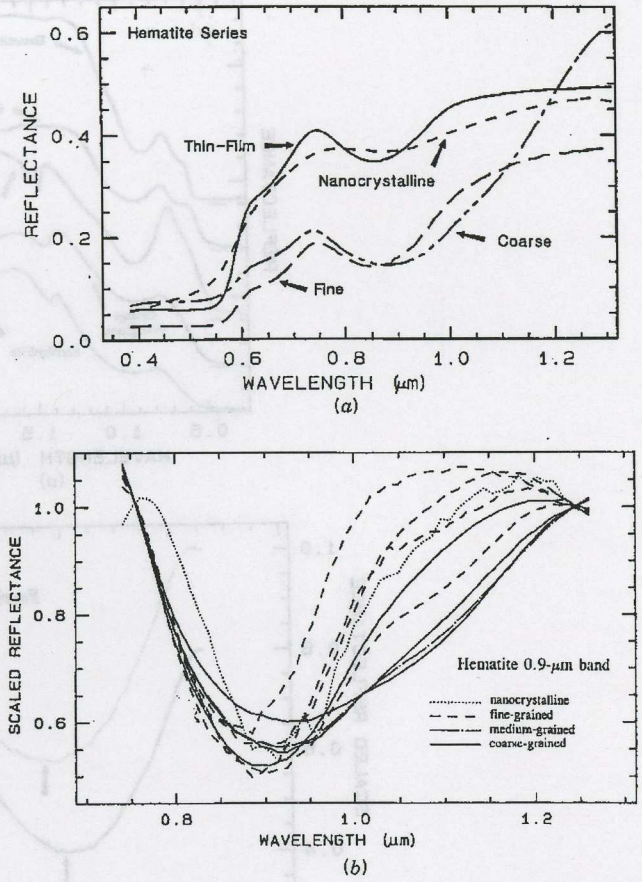

Figure 1.29 (*a*) Reflectance spectra of different grain sizes of hematite; (*b*) continuum-removed reflectance spectra different grain sizes of hematite.

Iron oxides, hydroxides, and sulfates are additional cases where spectroscopy tects at very low levels because of the strong absorption bands in the visible a ultraviolet. In nature, there appear to be many amorphous iron oxides, hydroxid and so on, with equally intense absorptions. Thus spectroscopy cannot only det them at levels below other methods (e.g., x-ray diffraction), but in the case of am phous materials can detect them when other methods are not sensitive to their pr ence when they are major fractions of the sample!

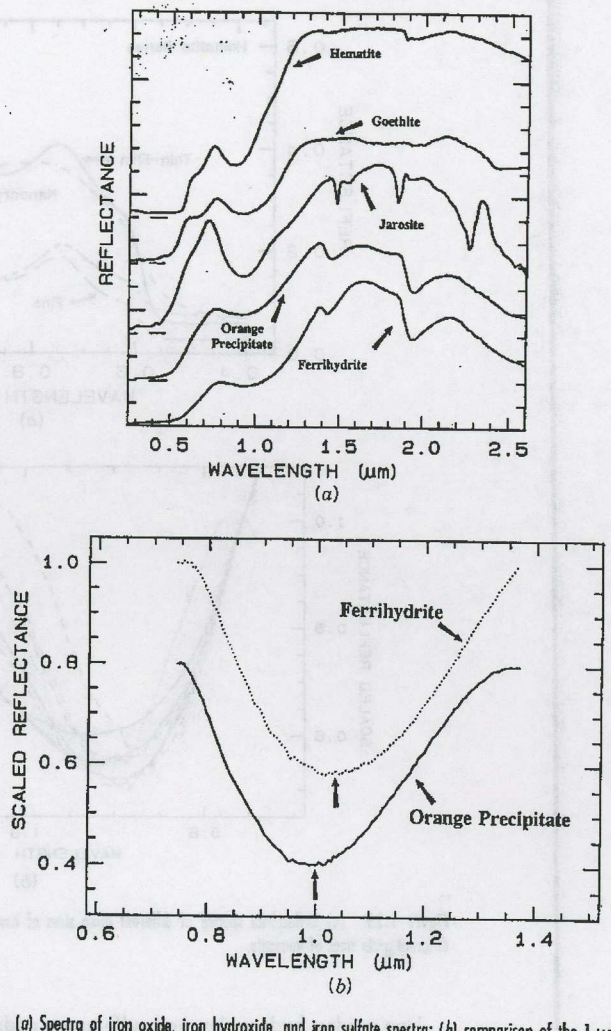

Figure 1.30 (*a*) Spectra of iron oxide, iron hydroxide, and iron sulfate spectra; (*b*) comparison of the 1-μm continuum-removed absorption feature of ferrihydrite and an amorphous iron hydroxide [the orange precipitate from part (*a*)]. The spectra are offset for clarity. Note the shift in the band center between the two spectra despite the similarities in part (*a*).

1.7 QUANTITATIVE UNDERSTANDING: RADIATIVE TRANSFER THEORY

There have been many attempts over the years to quantify the scattering proce Kubelka–Munk theory was one of the first and still finds uses today (e.g., Wendla and Hecht, 1966; Clark and Roush, 1984). A method growing in popularity in so industries is log (1/*R*), where *R* is reflectance, but this is a less robust attempt quantifying the scattering process than the decades-old Kubelka–Munk theory (Cl and Roush, 1984). The latter method is usually combined with computing the rivatives of the log (1/*R*) spectra and doing a correlation analysis to find particu trends. This has popularly become known as *near-infrared reflectance analy* (NIRA). Either method has its uses in controlled situations, but there is a mode more effective alternative. The limitations of these older methods are due to a po representation of the scattering process and are discussed in Clark and Roush (198 and Hapke (1993).

Fortunately, in the early 1980s three independent investigations (Hapke, 198 Goguen, 1981; Lumme and Bowell, 1981) provided reasonable solutions to the co plex radiative transfer problem as applied to particulate surfaces. These theor provide for nonisotropic scattering of light from particles, shadowing between p ticles, and first surface reflection from grain surfaces, important processes not co sidered in earlier theories. One theory, that of Hapke (1981, 1993), also provid for mixtures, and because of its relative simplicity compared to the other two, h become the dominant theory used in the planetary and to some degree the terrestr remote sensing communities.

1.7.1 Hapke Theory

From the optical constants of a mineral, the reflectance (called the *radiance fact* by Hapke) can be computed from Hapke's (1981) eq. 36:

$$r'(\bar{w}, \lambda, \mu, g) = \frac{\bar{w}}{4\pi} \frac{\mu}{\mu + \mu_0} \{[1 + B(g)]P(g) + H(\mu)H(\mu_0) - 1\} \qquad (1.$$

where r' is the reflectance at wavelength λ, $\bar{w}$ the average single scattering albedo, the cosine of the angle of emitted light, g the phase angle, μ_0 the cosine of the ang of incident light, $B(g)$ a backscatter function, $P(g)$ the average single-particle pha function, and H the Chandrasekhar (1960) H-function for isotropic scatterers. Wh $r' > 0.9$ Hapke's approximation of the H-function shows considerable error a equation (1.7) deviates from measurements (Hapke, 1981). Because of this deviatio a table interpolation subroutine using "exact" values from Chandrasekhar (196 can be used. The table interpolation is faster computationally than the Hapke a proximation, as well as being more accurate.

The single-scattering albedo is the probability that a photon survives an intera tion with a single particle, which includes Fresnel reflection, absorption, scatterin and diffraction due to the presence of an individual grain. Hapke (1981) develop the theory further by deriving a relation between the single-scattering albedo, t

complex index of refraction, the grain size, and a scattering parameter to describe scattering centers within nonperfect grains. The single-scattering albedo of a grain can be found from his eq. 24:

$$w = S_E + \frac{(1 - S_E)(1 + S_I)(r_1 + \exp[-2(k(k + s))^{1/2}d/3])}{1 - r_1 S_I + (r_1 - S_i)\exp[-2(k(k + s))^{1/2}d/3]} \quad (1.8)$$

where S_E and S_I are the external and internal scattering coefficients, respectively, which can be computed from the complex index of refraction (Hapke, 1981, eq. 21), s is a scattering coefficient, d is the particle diameter, k is the absorption coefficient (note that Hapke uses α instead of k here), and (from Hapke's eq. 23)

$$r_1 = \frac{1 - [k/(k + s)]^{1/2}}{1 + [k/(k + s)]^{1/2}} = \frac{1 - [kd/(kd + sd)]^{1/2}}{1 + [kd/(kd + sd)]^{1/2}} \quad (1.9)$$

In a monomineralic surface, $w = \bar{w}$. For a multimineralic surface, $\bar{w}$ can be computed from eq. 17 of Hapke (1981):

$$\bar{w} = \frac{\sum_i \frac{M_i w_i}{\rho_i d_i}}{\sum_i \frac{M_i}{\rho_i d_i}} \quad (1.10)$$

where i refers to the ith component, M_i is the mass fraction, w_i the single-scattering albedo of the ith component, ρ_i the density of the material, and d_i the mean grain diameter.

With the Hapke (1981, 1993) reflectance theory and the optical constants of minerals, reflectance spectra of pure minerals at a single grain size, spectra of a pure mineral with a grain size distribution, and mineral mixtures with varying grain size components can all be computed. Clark and Roush (1984) also showed that a reflectance spectrum can be inverted to determine quantitative information on the abundances and grain sizes of each component. The inversion of reflectance to quantitative abundance has been tested in laboratory mixtures (e.g., Johnson et al., 1983, 1992; Clark, 1983; Mustard and Pieters, 1987a, 1989; Shipman and Adams, 1987; Sunshine and Pieters, 1990, 1991; Sunshine et al., 1990; Gaffey et al., 1993; and references therein). Some quantitative inversion attempts have been undertaken with imaging spectroscopy data (e.g., Mustard and Pieters, 1987b; Adams et al., 1993; Li et al., 1996; and references therein).

1.8 SPECTRAL LIBRARIES

The spectra presented in this paper are available on the World Wide Web site http://speclab.cr.usgs.gov, as are spectra from the Clark et al. (1993b) USGS digital spectral library. Other spectral libraries include the mid-infrared work of Salisbury et al. (1991). A recently available spectral library Web site is the NASA ASTER site (http://asterweb.jpl.nasa.gov), managed by Simon Hook, Jet Propulsion Laboratory. This

site includes the Salisbury et al. (1991) library and additions since the original pu
lication. As spectral libraries are currently a focus of activity, it is probably best
search the Internet and check with the authors cited in this chapter for the lat
information on what is available.

A word of caution concerning spectral libraries and spectra obtained from oth
sources in general: Wavelength errors are common except from data obtained
interferometers. This author and colleagues at the USGS have evaluated many sp
trometers and other spectral libraries and have found many to have significant wa
length shifts. Other specific libraries and spectrometers are not mentioned here
cause some may have wavelength shifts and must each be validated. One mine
with a stable absorption feature is a well-crystallized kaolinite which has a sha
absorption at 2.2086 ± 0.0003 μm and is commonly found in visible and ne
infrared libraries. When obtaining spectral library data, confirm that wavelen
positions of known features are measured at the correct positions. Absorptions d
to rare earth oxides are often used as wavelength standards in the visible. M
infrared systems can be checked by interferometer measurements, which is now pro
ably the most common spectrometer in use for this wavelength region.

Also be cautious of spurious spectral features from incomplete reduction to tr
reflectance. All measurements are made relative to a "white" standard. Howev
these standards also have spectral features. For example, the common visible a
near-infrared standards, Halon and Spectralon and derivatives, have significant sp
tral features in the 2.14-μm region and beyond (see, e.g., Clark et al., 1990a) whi
must be corrected properly. Mid-infrared standards are more difficult, due primar
to the wide wavelength range usually covered. Nash (1986) reviewed some comm
mid-infrared reflectance standards.

1.9 CONCLUSIONS AND DISCUSSION

Reflectance spectroscopy is a rapidly growing science that can be used to deri
significant information about mineralogy with little or no sample preparation. It m
be used in applications when other methods would be too time consuming or requi
destruction of precious samples. For example, imaging spectrometers are alrea
acquiring millions of spatially gridded spectra over an area from which mineralogi
maps are being made. It is possible to set up real-time monitoring of processes usi
spectroscopy, such as monitoring the mineralogy of drill cores at the drilling si
Research is still needed to better understand the subtle changes in absorption featu
before reflectance spectroscopy will reach its full potential. Good spectral databas
documenting all the absorption features are also needed before reflectance spectro
copy can be as widely used as XRD. Spectral databases are now becoming availab
(e.g., Clark et al., 1993b) and research continues on the spectral properties of mi
erals, but it will probably take about a decade before general software tools a
available to allow reflectance spectroscopy to challenge other analytical methods
the commercial marketplace. For certain classes of minerals, however, spectrosco
is already an excellent tool. Among these classes are clay mineralogy, OH-beari
minerals, iron oxides and hydroxides, carbonates, sulfates, olivines, and pyroxen

Space limits the contents of any review article covering such a broad topic. Oth
review articles are Adams (1975), Hunt (1977, 1982), Gaffey et al. (1993), Salisbu

(1993), and Clark (1995). The Hunt (1982) article in particular presents more spectra, both visible–near-infrared and mid-infrared, than most other works and seems to be an overlooked but important work.

ACKNOWLEDGMENTS

This work was supported by NASA interagency agreement W15805. Thanks goes to reviewers John Mustard, Gregg Swayze, and Eric Livo, whose comments improved the manuscript substantially.

References

Adams, J. B., 1974. Visible and near-infrared diffuse reflectance spectra of pyroxene and applied to remote sensing of solid objects in the solar system, *J. Geophys Res.*, 79, 4829–4836.

Adams, J. B., 1975. Interpretation of visible and near-infrared diffuse reflectanc spectra of pyroxenes and other rock-forming minerals, in *Infrared and Rama Spectroscopy of Lunar and Terrestrial Minerals*, C. Karr, ed., Academic Press, Sa Diego, Calif., pp. 94–116.

Adams, J. B., M. O. Smith, and A. R. Gillespie, 1993. Imaging spectroscopy: inter pretation based on spectral mixture analysis, in *Remote Geochemical Analysi Elemental and Mineralogical Composition*, C. M. Pieters and P. A. J. Englert, eds Cambridge University Press, Cambridge, pp. 145–166.

Ball, D. W., 1995. Defining terms, *Spectroscopy*, 10, 16–18.

Berk, A., L. S. Bernstein, and D. C. Robertson, 1989. *MODTRAN: A Moderat Resolution Model for LOWTRAN 7, Final Report*, AFGL-TR-0122, Air Forc Geophysics Laboratory, Hanscomb AFB, Mass., 42 pp.

Burns, R., 1970. *Mineralogical Applications of Crystal Field Theory*, Cambridg University Press, Cambridge, 224 pp.

Burns, R., 1993. *Mineralogical Applications of Crystal Field Theory*, 2nd ed., Can bridge University Press, Cambridge, 551 pp.

Chandrasekhar, S., 1960. *Radiative Transfer*, Dover, Mineola, N.Y. 393 pp.

Clark, R. N., 1981a. Water frost and ice: the near-infrared spectral reflectance 0.65 2.5 μm, *J. Geophys. Res.*, 86, 3087–3096.

Clark, R. N., 1981b. The spectral reflectance of water–mineral mixtures at low tem peratures, *J. Geophys. Res.*, 86, 3074–3086.

Clark, R. N., 1983. Spectral properties of mixtures of montmorillonite and dar carbon grains: implications for remote sensing minerals containing chemically an physically adsorbed water, *J. Geophys. Res.*, 88, 10635–10644.

Clark, R. N., 1995. Reflectance spectra, in *AGU Handbook of Physical Constant* American Geophysical Union, Washington, D.C., 12 pp.

Clark, R. N., and T. V. V. King, 1987. Causes of spurious features in spectral r flectance data, in *Proceedings of the 3rd Airborne Imaging Spectrometer Da Analysis Workshop*, JPL Publ. 87–30, Jet Propulsion Laboratory, California I stitute of Technology, Pasadena, Calif., pp. 132–137.

Clark, R. N., and P. G. Lucey, 1984. Spectral properties of ice–particulate mixtures and implications for remote sensing: I. Intimate mixtures, *J. Geophys. Res.*, 89, 6341–6348.

Clark, R. N., and T. L. Roush, 1984. Reflectance spectroscopy: quantitative analysis techniques for remote sensing applications, *J. Geophys. Res.*, 89, 6329–6340.

Clark, R. N., F. P. Fanale, and M. J. Gaffey, 1986. Surface composition of satellites, in *Natural Satellites*, J. Burns and M. S. Matthews, eds., University of Arizona Press, Tucson, Ariz., pp. 437–491.

Clark, R. N., T. V. V. King, M. Klejwa, G. Swayze, and N. Vergo, 1990a. High spectral resolution reflectance spectroscopy of minerals, *J. Geophys. Res.*, 95, 12653–12680.

Clark, R. N., A. J. Gallagher, and G. A. Swayze, 1990b. Material absorption band depth mapping of imaging spectrometer data using a complete band shape least-squares fit with library reference spectra, in *Proceedings of the 2nd Airborne Visible/Infrared Imaging Spectrometer (AVIRIS) Workshop*, JPL Publ. 90–54, Jet Propulsion Laboratory, California Institute of Technology, Pasadena, Calif., pp. 176–186.

Clark, R. N., G. A. Swayze, and A. Gallagher, 1993a. *Mapping Minerals with Imaging Spectroscopy*, USGS Bull. 2039, U.S. Geological Survey, Office of Mineral Resources, Washington, D.C., pp. 141–150.

Clark, R. N., G. A. Swayze, A. Gallagher, T. V. V. King, and W. M. Calvin, 1993b. *The U.S. Geological Survey, Digital Spectral Library, Version 1: 0.2 to 3.0 μm*, USGS Open File Rep. 93–592, U.S. Geological Survey, Washington, D.C., 1326 pp.

Clark, R. N., T. V. V. King, C. Ager, and G. A. Swayze, 1995. Initial vegetation species and senescence/stress mapping in the San Luis Valley, Colorado using imaging spectrometer data, in *Proceedings of the Summitville Forum '95*, H. H. Posey, J. A. Pendelton, and D. Van Zyl, eds., CGS Spec. Publ. 38, Colorado Geological Survey, Colo., pp. 64–69.

Clark, R. N., T. V. V. King, C. Ager, and G. A. Swayze, submitted. Vegetation species and stress indicator mapping in the San Luis Valley, Colorado using imaging spectrometer data, *Remote Sensing Environ.* 1998.

Cloutis, E. A., and M. J. Gaffey, 1991. Pyroxene spectroscopy revisited: spectral–compositional correlations and relationships to geothermometry, *J. Geophys. Res.*, 96, 22809–22826.

Cloutis, E. A., M. J. Gaffey, T. L. Jackowski, and K. L. Reed, 1986. Calibrations of phase abundance, composition, and particle size distribution of olivine–orthopyroxene mixtures from reflectance spectra, *J. Geophys. Res.*, 91, 11641–11653.

Crowley, J. K., and N. Vergo, 1988. Near-infrared reflectance spectra of mixtures of kaolin group minerals: use in clay studies, *Clays Clay Miner.*, 36, 310–316.

Cruikshank, D. P., R. H. Brown, and R. N. Clark, 1985. Methane ice on Triton and Pluto, in *Ices in the Solar System*, J. Klinger et al., eds., D. Reidel, Dordrecht, The Netherlands, pp. 817–827.

Duke, E. F., 1994. Near infrared spectra of muscovite, Tschermak substitution, and metamorphic reaction progress: implications for remote sensing, *Geology*, 22, 621–624.

Farmer, V. C., ed., 1974. *The Infra-red Spectra of Minerals*, Mineralogical Society, London, 539 pp.

Gaffey, S. J., 1986. Spectral reflectance of carbonate minerals in the visible and ne infrared (0.35–2.55 μm): calcite, aragonite and dolomite, *Am. Mineral.*, 71, 15 162.

Gaffey, S. J., 1987. Spectral reflectance of carbonate minerals in the visible and ne infrared (0.35–2.55 μm): anhydrous carbonate minerals, *J. Geophys. Res.*, 9 1429–1440.

Gaffey, S. J., L. A. McFadden, D. Nash, and C. M. Pieters, 1993. Ultraviolet, visib and near-infrared reflectance spectroscopy: laboratory spectra of geologic mat rials, in *Remote Geochemical Analysis: Elemental and Mineralogical Compo tion*, C. M. Pieters, and P. A. J. Englert, eds., Cambridge University Press, Ca bridge, pp. 43–78.

Goetz, A. F. H, G. Vane, J. E. Solomon, and B. N. Rock, 1985. Imaging spectromet for earth remote sensing, *Science*, 228, 1147–1153.

Goguen, J. D., 1981. A theoretical and experimental investigation of the photom ric functions of particulate surfaces, Ph.D. thesis, Cornell University, Ithac N.Y.

Green, R. O., J. E. Conel, V. Carrere, C. J. Bruegge, J. S. Margolis, M. Rast, and Hoover, 1990. Determination of the in-flight spectral and radiometric charact istics of the airborne visible/infrared imaging spectrometer (AVIRIS), in *Proce ings of the 2nd Airborne Visible/Infrared Imaging Spectrometer (AVIRIS) Wor shop*, JPL Publ. 90–54, Jet Propulsion Laboratory, California Institute Technology, Pasadena, Calif., pp. 15–22.

Hapke, B., 1981. Bidirectional reflectance spectroscopy: 1. Theory, *J. Geophys. Re* 86, 3039–3054.

Hapke, B., 1993. *Introduction to the Theory of Reflectance and Emittance Spe troscopy*, Cambridge University Press, New York.

Hecht, E., 1987. *Optics*, Addison-Wesley, Reading Mass., 676 pp.

Henderson, B. G., P. G. Lucey, and B. M. Jakosky, 1996. New laboratory measu ments of mid-IR emission spectra of simulated planetary surfaces, *J. Geophy Res.*, 101, 14969–14975.

Herzberg, G., 1945. *Molecular Spectra and Molecular Structure, Vol. 2, Infrared a Raman Spectra of Polyatomic Molecules*, Van Nostrand Reinhold, New Yo 632 pp.

Hobbs, P. V., 1974. *Ice Physics*, Clarendon Press, Oxford, 837 pp.

Hunt, G. R., 1977. Spectral signatures of particulate minerals, in the visible and nea infrared, *Geophysics*, 42, 501–513.

Hunt, G. R., 1979. Near-infrared (1.3–2.4 μm) spectra of alteration minerals: p tential for use in remote sensing, *Geophysics*, 44, 1974–1986.

Hunt, G. R., 1982. Spectroscopic properties of rocks and minerals, in *Handbook Physical Properties of Rocks*, Vol. 1, R. S. Carmichael, ed., CRC Press, Boca R ton, Fla., pp. 295–385.

Hunt, G. R., and J. W. Salisbury, 1970. Visible and near infrared spectra of miner and rocks: I. Silicate minerals, *Mod. Geol.*, 1, 283–300.

Hunt, G. R., and J. W. Salisbury, 1971. Visible and near infrared spectra of miner and rocks: II. Carbonates, *Mod. Geol.*, 2, 23–30.

Hunt, G. R., J. W. Salisbury, and C. J. Lenhoff, 1971a. Visible and near infrar spectra of minerals and rocks: III. Oxides and hydroxides, *Mod. Geol.*, 2, 19 205.

Hunt, G. R., J. W. Salisbury, and C. J. Lenhoff, 1971b. Visible and near infrared spectra of minerals and rocks: IV. Sulphides and sulphates, *Mod. Geol.*, 3, 1–14.

Hunt, G. R., J. W. Salisbury, and C. J. Lenhoff, 1972. Visible and near infrared spectra of minerals and rocks: V. Halides, arsenates, vanadates, and borates, *Mod. Geol.*, 3, 121–132.

Hunt, G. R., J. W. Salisbury, and C. J. Lenhoff, 1973. Visible and near infrared spectra of minerals and rocks: VI. Additional silicates, *Mod. Geol.*, 4, 85–106.

Johnson, P., M. Smith, and S. Taylor-George, 1983. A semi-empirical method for analysis of the reflectance spectra of binary mineral mixtures, *J. Geophys. Res.*, 88, 3557–3561.

Johnson, P. M., M. O. Smith, and J. B. Adams, 1992. Simple algorithms for remote determination of mineral abundances and particle sizes from reflectance spectra, *J. Geophys. Res.*, 97, 2649–2657.

King, T. V. V., and R. N. Clark, 1989a. Spectral characteristics of serpentines and chlorites using high resolution reflectance spectroscopy, *J. Geophys. Res.*, 94, 13997–14008a.

King, T. V. V., and R. N. Clark, 1989b. Reflectance spectroscopy (0.2 to 20μm) as an analytical method for the detection of organics in soils; in *Proceedings of the First International Symposium: Field Screening Methods for Hazardous Waste Site Investigations*, U.S. Environmental Protection Agency, Washington, D.C., pp. 485–488.

King, T. V. V., and W. I. Ridley, 1987. Relation of the spectroscopic reflectance of olivine to mineral chemistry and some remote sensing implications, *J. Geophys. Res.*, 92, 11457–11469.

King, T. V. V., R. N. Clark, C. Ager, and G. A. Swayze, 1995. Remote mineral mapping using AVIRIS data at Summitville, Colorado and the adjacent San Juan Mountains, in *Proceedings of the Summitville Forum '95*, H. H. Posey, J. A. Pendelton, and D. Van Zyl eds., CGS Spec. Publ. 38, Colorado Geological Survey, Boulder, Colo., pp. 59–63.

Li, L., J. F. Mustard, and G. He, 1996. Mixing across simple mare–highland contacts: new insights from *Clementine* UV–VIS data of the Grimaldi basin, in *Lunar and Planetary Science XXVII*, Lunar and Planetary Institute, Houston, Texas, pp. 751–752.

Lucey, P. G., and R. N. Clark, 1985. Spectral properties of water ice and contaminants, in *Ices in the Solar System*, J. Klinger et al., eds., D. Reidel, Dordrecht, The Netherlands, pp. 155–168.

Lumme, K., and Bowell, E., 1981. Radiative transfer in the surfaces of atmosphereless bodies: I. Theory, *Astron. J.*, 86, 1694–1704.

Morris, R. V., H. V. Lauer, C. A. Lawson, E. K. Gibson, Jr., G. A. Nace, and C. Stewart, 1985. Spectral and other physiochemical properties of submicron powders of hematite (α-Fe_2O_3), maghemite (γ-Fe_2O_3), maghemite (Fe_3O_4), goethite (α-FeOOH), and lepidochrosite (γ-FeOOH), *J. Geophys. Res.*, 90, 3126–3144.

Mustard, J. F., 1992. Chemical composition of actinolite from reflectance spectra, *Am. Mineral.*, 77, 345–358.

Mustard, J. F., and C. M. Pieters, 1987a. Quantitative abundance estimates from bidirectional reflectance measurements, in *Proceedings of the 17th Lunar and Planetary Science Conference, J. Geophys. Res.*, 92, E617–E626.

Mustard, J. F., and C. M. Pieters, 1987b. Abundance and distribution of serpentinized ultramafic microbreccia in Moses Rock dike: quantitative application of ma
ping spectrometer data, *J. Geophys. Res.*, 92, 10376–10390.

Mustard, J. F., and C. M. Pieters, 1989. Photometric phase functions of comm
geologic minerals and applications to quantitative analysis of mineral mixtu
reflectance spectra, *J. Geophys. Res.*, 94, 13619–13634.

Nash, D. B., 1986. Mid-infrared reflectance spectra (2.3–22 μm) of sulfur, gold, FE
Mgo and Halon, *Appl. Opt.*, 25, 2427–2433.

Nelson, M. L., 1986. Application of radiative transfer theory to the spectra
mixtures of minerals with anisotropic phase functions, Master's thesis, Universi
of Hawaii, Honolulu, Hawaii, 71 pp.

Nicodemus, F. E., 1965. Directional reflectance and emissivity of an opaque surfac
Appl. Opt., 4, 767–773.

Post, J. L., and P. N. Noble, 1993. The near-infrared combination band frequenci
of dioctahedral smectites, micas, and illites, *Clays Clay Miner.*, 41, 639–644.

Salisbury, J. W., 1993. Mid-infrared spectroscopy: laboratory data, in *Remote G
ochemical Analysis: Elemental and Mineralogical Composition*, C. M. Pieters a
P. A. J. Englert, eds., Cambridge University Press, Cambridge, pp. 79–98.

Salsibury, J. W., L. S. Walter, N. Vergo, and D. M. D'Aria, 1991. *Infrared (2.1–2
μm) Spectra of Minerals*, Johns Hopkins University Press, Baltimore, 267 pp.

Sherman, D. M., 1990. Crystal chemistry, electronic structures and spectra of Fe sit
in clay minerals, in *Spectroscopic Characterization of Minerals and Their Surfac
L. M. Coyne, S. W. S. McKeever, and D. F. Drake, eds., American Chemical S
ciety, Washington, D.C., pp. 284–309.

Shipman, H., and J. B. Adams, 1987. Detectability of minerals on desert alluvial fa
using reflectance spectra, *J. Geophys. Res.*, 92, 10391–10402.

Spitzer, W. G., and D. A. Kleinman, 1960. Infrared lattice bands of quartz, *Phy
Rev.*, 121, 1324–1335.

Sunshine, J. M., and C. M. Pieters, 1990. Extraction of compositional informati
from olivine reflectance spectra: new capability for lunar exploration (abstrac
in *Lunar and Planetary Science XXI*, Lunar and Planetary Institute, Housto
Texas, pp. 962–963.

Sunshine, J. M., and C. M. Pieters, 1991. Identification of modal abundances in spe
tra of natural and laboratory pyroxene mixtures: a key component for remo
analysis of lunar basalts (abstract), in *Lunar and Planetary Science XXII*, Lun
and Planetary Institute, Houston, Texas, pp. 1361–1362.

Sunshine, J. M., and C. M. Pieters, and S. R. Pratt, 1990. Deconvolution of miner
absorption bands: an improved approach, *J. Geophys. Res.*, 95, 6955–6966.

Swayze, G. A., 1997. The hydrothermal and structural history of the Cuprite mini
district, southwestern Nevada: an integrated geological and geophysical approac
Ph.D. dissertation, University of Colorado at Boulder, Boulder, Colo., 430 pp.

Swayze, G. A., and R. N. Clark, 1990. Infrared spectra and crystal chemistry
scapolites: implications for Martian mineralogy, *J. Geophys. Res.*, 95, 1448
14495.

Swayze, G. A., R. N. Clark, A. F. H Goetz, N. S. Gorelick, and T. G. Chrien, su
mitted. Spectral identification of surface materials using imaging spectrome
data: evaluating the effects of detector sampling, bandpass, and signal to noi
ratio using the U.S.G.S. Tetracorder algorithm: Parts I and II, *J. Geophys. Res.*

Vane, G., J. E. Duval, and J. B. Wellman, 1993. Imaging spectroscopy of the Ear

and other solar system bodies, in *Remote Geochemical Analysis: Elemental and Mineralogical Composition*, C. M. Pieters and P. A. J. Englert, eds., Cambridge University Press, Cambridge, pp. 121–143.

Wendlandt, W. W., and H. G. Hecht, 1966. *Reflectance Spectroscopy*, Interscience, New York, 298 pp.

White, W. B., 1974. The carbonate minerals, in *The Infrared Spectra of Minerals*, V. C. Farmer, ed., Mineralogical Society, London, pp. 227–284.

Chapte

2

Use of Multispectral Thermal Infrared Dat in Geological Studie

Simon J. Hook, Elsa A. Abbott, C. Grove A. B. Kahle, and F. Pallucon

California Institute of Technolo
Pasadena, CA 911

2.1 INTRODUCTION

Mineral spectra exhibit diagnostic features at various wavelengths which provide means for their remote discrimination and identification. These features are produc by electronic or vibrational–rotational processes resulting from the interaction electromagnetic energy with the atoms and molecules which comprise the minera that make up a rock. The different processes require different amounts of energy proceed, and therefore are manifest in different wavelength regions. Electronic pro esses require the most energy and result in spectral features in the visible and nea infrared wavelength regions. Fundamental vibrational processes require less energ and evidence for them occurs beyond 2.5 μm. Between 0.5 and 2.5 μm there is overlap of features due to electronic processes and the excitation of overtone a combination-tone vibrations (Hunt, 1980).

Iron-, hydroxyl-, water-, sulfate-, and carbonate-bearing minerals display spectr features in the wavelength region 0.4 to 2.5 μm (Figure 2.1). By contrast, silica minerals such as quartz, which dominate most crustal rocks, exhibit spectral featu

Remote Sensing for the Earth Sciences: Manual of Remote Sensing, 3 ed., Vol. 3, edited by Andrew Rencz.
ISBN: 0471-29405-5